Electronic excitations, spectroscopy and quantum transport from ab initio theory

Valerio Olevano

Electronic excitations, spectroscopy and quantum transport from *ab initio* theory

Valerio Olevano

Institut Néel, CNRS & Université Joseph Fourier, Grenoble

September 22, 2009

Abstract

Spectroscopy and quantum transport constitute powerful ways to study the physics of matter and to access the electronic and atomic structure. Excitations, in turn determined by the electronic and atomic structure, lie at the origin of spectroscopy and quantum transport. *Ab initio* calculation of excited states requires to go beyond ground-state density-functional theory (DFT).

In this work we review three theoretical frameworks beyond DFT: the first is time-dependent density-functional theory to describe neutral excitations and to address energy-loss and optical spectroscopies. We introduce the theory and the fundamental approximations, i.e. the RPA and the adiabatic LDA, together with the results one can get with them at the example of bulk silicon and graphite. We then describe the developments we contributed to the theory beyond TDLDA to better describe optical spectroscopy, in particular the long-range contribution-only and the Nanoquanta exchange-correlation kernel approximations.

The second framework is many-body quantum field theory (or Green's function theory) in the GW approximation and beyond, well suited to describe photoemission spectroscopy. After a review of the theory and its main success on the prediction of the band gap, we present two applications on unconventional systems: 2D graphene and strongly correlated vanadium dioxide. We discuss the next frontiers of GW, closing with perspectives beyond GW and MBQFT.

The last part presents non-equilibrium Green's function theory suited to address quantum transport. We show how it reduces to the state-of-the-art Landauer principal layers framework when neglecting correlations. We present a calculation of the conductance on a very simple system, a gold monoatomic chain, showing the effect of electron-electron scattering effects. Finally we present theoretical developments toward a new workbench beyond the principal layers, which led us to the introduction of new generalized Meir and Wingreen and Fisher-Lee formulas.

This work compares the theoretical and practical aspects of both Green's function and density based approaches, each one benefiting insights from the other, and presents an overview of accomplishments and perspectives.

Contents

Introduction

Spectroscopy constitutes today for the experiment one of the most powerful way to access and study the physics of condensed matter. Excitations lie at the origin of any spectroscopy. Every spectroscopy experiment measures the response of a system to an external perturbation. External incoming photons, electrons, etc. perturbe the system from its initial state and excite it to another state. The response to the perturbation is hence related to the excitations the system undergoes. By measuring the response and with a knowledge of the perturbation, one can extract important informations about the excitations and hence about the electronic and atomic structure of the system.

In this work we will focus in particular on electronic excitations and spectroscopies related to them. Photoemission, optical absortion and energy-loss can be taken as prototype spectroscopies in this context. Aside, we will also consider quantum transport that, dependending on the definition, can be considered a spectroscopy in itself (one measures the current in response to an applied bias). In all these cases, in order to describe, reproduce, interpret or even predict a spectrum, it is fundamental to have an accurate and precise description of excitations, in turn determined by the electronic and atomic structure of the system which is hence the main problem stated to the theory.

For the interpretation of a spectrum one can already be satisfied with a more or less simple adjustable-parameters model which tries to capture the main physics behind observed phenomena. The model can go from a simple fit of the spectrum by a collection of lorentzians/gaussians, as we did for example in Ref.s [Battistoni 96, Galdikas 97] to interpret photoemission and Auger spectra. To a more physical model that tries to speculate on the microscopic nature of the system, presenting what is guessed to be the most relevant physics to explain phenomena and neglect the rest. This represents an *a priori* conjecture done at the very beginning and which can reveal true or false. In the latter case it leads to a completely wrong interpretation of phenomena. Moreover, a model always presents few or many parameters to be adjusted on the experiment. For this reason it can never achieve the rank of a "predictive theory" in a scientific and *epistemological* sense.

For all these reasons, it would be extremely desirable to have a description of the atomic and electronic structure, of excitations and finally of spectroscopy by a microscopical *ab initio* theory. Such a *first principles* theory should possibly take into account all the microscopic degrees of freedom of the system and consider the full Hamiltonian presenting the real interactions of nature. The advantage of an *ab initio* theory is that it does not rely on a conjecture which may completely falsify the conclusions about the intepretation of a phenomenon. Further on, since it does not rely on adjustable parameters, an *ab initio* the-

ory can lead to "prediction", which is a fundamental aspect of the scientific methodology since Galileo.

The problem in physics of matter is that even the simplest systems present an enormous level of complexity. Exact analytic solutions are known only in few and very simple real systems, such as hydrogen and hydrogenoid atoms. Problems start to appear already for the helium atom, a two-electron system. In any case, the follow up of all the degrees of freedom cannot be normally accomplished in an analytic way. Computer calculations are unavoidable to describe real condensed matter systems. Although *ab initio* theories try to keep as much as possible exact in principle, in almost all the cases approximations are required to achieve a result, either for missing knowledge of key quantities of the theory or for numerical unfeasibility. Of course, approximations are avoided for all the quantities which can be calculated exactly, and their application is as much as possible delayed to the last calculation steps. However, approximations for which an *a priori* evaluation of the error is possible like for example in perturbation theory, are seldom in condensed matter theory. The quality of an approximation cannot in many cases be stated in advance, and only heuristic considerations are possible. Most of them can only be validated *a posteriori*, after having accumulated a large statistics on systems. Such a state of affairs and all these difficulties can be traced back and derive from one, although severe, complication of condensed matter theory: the so-called "many-body problem". This is the real "guilty", responsible of most of the difficulties encountered by condensed matter theory in the purpose to describe the atomic and the electronic structure, as well as all physical properties related to them. Its statement will be exposed in the next section and the various proposed solutions constitute the main argument of this manuscript and the basic motivation of all my research work so far.

This work is organized in the following way: in the first chapter we introduce the many-body problem and the most important theories proposed to tackle it, namely many-body quantum field theory (MBQFT), also known as Green's function theory, and density-functional theory. Chapter 2 will present time-dependent density-functional theory (TDDFT) together with our personal contributions to the development of new approximations within TDDFT, in order to address not only energy-loss (EELS, IXSS) but also optical spectroscopies. The search for better approximations beyond the local-density has been the *leitmotiv* of my research activity since the PhD thesis work [Olevano 99b]. Chapter 3 will present MBQFT and the GW approximation, well suited to photoemission spectroscopy. Our recent contributions to the theory go toward the study of materials, like strongly correlated systems, where the quality of the GW approximation is seriously tested. We present also some new ideas with perspectives that go beyond not only GW but even MBQFT. The last chapter introduces non-equilibrium Green's function theory (NEGF) and its application to the quantum transport problem, together with our most recent contributions. As recommended for the achievement of a *Habilitation à Diriger des Recherches* degree of the Université Joseph Fourier, this work is written in a didactic form, *ad usum* of students starting their PhD on these arguments.

Chapter 1

The many-body problem and theories

1.1 The many-body problem

Let's take a generic condensed matter system containing N electrons. N can range from 1 (the hydrogen atom), to tens in atomic systems and simple molecules; up to the order of the Avogadro number $N_A \sim 10^{23}$ in solids. In the Born-Oppenheimer approximation, the Hamiltonian of the system can be written (atomic units, $m = e = \hbar = 1$, are assumed hereafter):

$$H = T + V + W = -\frac{1}{2}\sum_{n=1}^{N} \partial_{r_n}^2 + \sum_{n=1}^{N} v(r_n) + \frac{1}{2}\sum_{n\neq m=1}^{N} w(r_n, r_m), \qquad (1.1)$$

where $T = -1/2\sum_n \partial_{r_n}^2$ is the kinetic energy; $V = \sum_n v(r_n)$ is the external potential energy, the interaction of the electrons with an assumed external potential $v(r)$ due e.g. to ions supposed in fixed positions with respect to the electrons (Born-Oppenheimer approximation); and $W = 1/2\sum_{n\neq m} w(r_n, r_m)$ is the electron-electron interaction energy, that is the Coulomb repulsion

$$w(r, r') = \frac{1}{|r - r'|}$$

long range interaction among the N electrons of the system.

In an ideal case where the many-body electron-electron interaction $W = 0$ is switched off (this ideal system is called the independent-particle system and indicated with a superscript (0)), the Hamiltonian can be written

$$H^{(0)} = T + V = \sum_{n=1}^{N} h^{(0)}(r_n),$$

that is, it factorizes in N single-particle Hamiltonians,

$$h^{(0)}(r) = \left[-\frac{1}{2}\partial_r^2 + v(r)\right],$$

and the single-particle Schrödinger equation,

$$h^{(0)}(r)\phi_i^{(0)}(r) = \epsilon_i^{(0)}\phi_i^{(0)}(r),$$

can be easily solved to find the spectrum of the single-particle $\epsilon_i^{(0)}$ eigenenergies and $\phi_i^{(0)}(r)$ eigenfunctions. The solutions to the Schrödinger equation of the total N electrons system,

$$H^{(0)}\Phi_i^{(0)}(r_1,\ldots,r_N) = E_i^{(0)}\Phi_i^{(0)}(r_1,\ldots,r_N),$$

can then be easily written in terms of the single-particle spectrum. In particular, keeping into account the fermionic nature of the N particles (the electrons) composing the system, the ground-state energy is

$$E_0^{(0)} = \sum_{n=1}^{N}\epsilon_n^{(0)},$$

and the ground-state wavefunction is the Slater determinant

$$\Phi_0^{(0)}(r_1,\ldots,r_N) = \frac{1}{\sqrt{N!}}\sum_P(-1)^P P\{\phi_i^{(0)}(r_n)\} \qquad i=1,N \quad n=1,N \quad (1.2)$$

(P is the permutation operator). The independent-particle approximation already provides an interesting physics. For instance, almost all the physics presented in condensed matter text books like Ref.s [Ashcroft 76, Kittel 66], is based on this approximation. The point is that the electron-electron repulsion is not an order of magnitude less than the electron-ion interaction expressed via the external potential. In a condensed matter system, positive and negative charges are usually compensated, or nearly, so that the external potential energy and the many-body interaction energy are of the same order. As we will show in the next, the independent-particle approximation reveals inappropriated in many cases. The problem is that when we try to reintroduce the many-body W term, the Hamiltonian is not any more factorizable and one should solve the full many-body Schrödinger equation,

$$H\Psi_i(r_1,\ldots,r_N) = E_i\Psi_i(r_1,\ldots,r_N), \quad (1.3)$$

which is a complicated problem even for a two-electron system, $N = 2$, like the helium atom. It becomes a formidable problem in macroscopic solids, where even just imaging to write the wavefunction $\Psi(r_1,\ldots,r_N)$, a function of $N \sim 10^{23}$ variables, is unaffordable.

This is known as the *many-body problem* and it is considered as one of the (if not "The") fundamental problem of condensed matter theoretical physics, as well as of other domains like theoretical nuclear (of the nuclei) physics. Starting from the '20s, several formalisms and theories have been proposed to tackle the problem. The first attempts were represented by the Hartree-Fock (HF) and Thomas-Fermi theories [Ashcroft 76, Kittel 66], well-known since taught in fundamental physics courses, but which were unable to provide a satisfying solution and are often very far from the experiment, apart from limited cases. The very final solution to the many-body problem cannot yet be considered

as found, but there have been important progresses. Efforts have been provided in particular toward two directions: the development of a quantum field theoretic and Green's function based formalism, known as *many-body quantum-field theory* (MBQFT), more frequently named *many-body perturbation theory* (MBPT); and the development of density-functional based theories, which led in particular to the succesful *density-functional theory* (DFT).

1.2 Many-body quantum field theory (MBQFT)

The many-body theory is a quantum field theoretic approach to the many-body problem. Quantum field theory is a formalism of quantum mechanics which relies on second quantization. The wavefunction $\psi(r)$ of ordinary quantum mechanics, which can be seen as a field over the space $r \in \mathbb{R}^3$, is itself quantized in the sense that it becomes a quantum (field) operator $\hat{\psi}(r)$.

This is a formalism largely developed in high-energy, particle and subnuclear physics where it gave rise to successful theories such as quantum electrodynamics (QED) to describe the electromagnetic interaction among particles, the electroweak theory, quantum chromodynamics (QCD), up to the standard model to describe weak and strong nuclear interactions in a unified picture with electromagnetism. In condensed matter physics, quantum field theory has been proposed since the sixties as promising candidate to the solution of the many-body problem. The advantages of a field theoretic treatement of the many-body problem are:

1. Second quantized operators avoid the need of indeces running on the entire set of particles composing a many-body system. As we have seen, particle indeces as in r_n, can run up to the Avagodro number in solid state physics.

2. Bosonic symmetrization or fermionic antisymmetrization of many-body wavefunctions are automatically imposed by second quantized operators. In first quantization, a many-body wavefunction $\Psi(r_1, \ldots, r_N)$ should be symmetrized by hands as for example in the construction (Eq. (1.2)) of a Slater determinant.

3. In a second quantization formalism it is possible to treat systems with varying number of particles. This is useful since condensed matter systems are not isolated but exchange with the rest of the universe. To treat these cases in a first quantization formalism, one should introduce potentials with an imaginary part.

4. Second quantization opens towards a Green's function formalism. On the basis of field operators, one can define a Green's function or propagator which reveals a quantity containing practically all the physical observables we are interested in, from the ground-state energy to excitations.

The latter is without doubt the most important point: in MBQFT the fundamental degree of freedom is not any more the complicated many-body wavefunction $\Psi(t, r_1, \ldots, r_N)$ of N variables, but rather the Green's function $G(r_1, t_1, r_2, t_2)$, which is a function of only two space-time variables. It is immediately evident how much more confortable is to handle Green's functions instead of many-body wavefunctions.

Following successful developments carried on for QED, it was hoped that also MBQFT could be expanded in perturbation theory toward checkable accuracy solutions to the many-body problem. So at the beginning a lot of efforts were given to the developpement of MBQFT in perturbation theory using Feynmann diagrams techniques. This is the reason why the theory is more known as many-body perturbation theory (MBPT). Sometime later it was however realized that the coupling constant of MBQFT is not small as in QED. Indeed in MBQFT one would like to consider as perturbation the complicated many-body term, which is unfortunately of the same order of the external potential term. The electron-electron interaction is not much smaller than the electron-ions interaction. A condensed matter system is normally neutral, that is it contains the same number of positive and negative charges. Hence it is not reasonable to consider the interaction among the electrons as second order with respect to the interaction between electrons and positive charges. In any case, formulation of MBQFT in perturbation theory gives back at the first order the Hartree-Fock theory, which is far to be a systematic good approximation. Since the coupling constant is not small, it is not granted that the second and further orders are smaller than the first. The perturbation series is not convergent and stopping at a given order is arbitrary.

The following orientations of the theory rather addressed toward partial resummations of the perturbation series along chosen directions. That is, a certain kind of Feynmann diagrams are summed up to infinity, in the hope to get the most important contribution. This is the sense of approximations like the random-phase approximation (RPA), which sums all the ring diagrams. Or the ladder approximation, for the ladder-like diagrams. Also these developments were more or less unsuccessful.

The developements of the theory followed at this point two main separate divergent research lines: the first line renounced to apply the theory to real systems, considered too complex, and rather focused to simple models. The initial hope was to achieve an analytical solution to the many-body problem for models and then, increasing the level of complexity, try to extend it to real systems. An analytical solution indeed is particularly valuable, since it allows to completely understand all the physics behind the system. The most studied models are the homogeneous electron gas (HEG), also known as jellium model, the largely spread Hubbard model, and others like the Andersson or the Kondo model. Unfortunately, although a lot of efforts have been devoted along this line, exact analytical solutions to these models are still unknown, apart from particular cases such as in 1 dimension, or for particular choices of the model adjustable parameters. Recent developments of this line desisted to achieve the exact analytical solution of models, and rather directed toward approximations and finally toward numerical solutions of models. One example of these developments is dynamical mean-field theory (DMFT) [Georges 96] that can provide an approximate and numerical solution to the Hubbard model. Having faced enormous difficulties to provide even approximate and numerical solutions to models, the hope then was that such models could somehow already represent real systems, or at least capture some isolated aspects of them. For example, the Hubbard model is believed to capture the physics of localized electrons such as the d or f electrons in transition metals or rare earth, and describe the so-called strongly-correlated physics in these systems.

The other main research line, instead, oriented since the beginning toward

providing a numerical solution to the many-body problem, although intrinsically less appealing than the analytical solution. Within the numerical line, several directions were taken: the quantum Montecarlo (QMC) approach addressed toward the achievement of numerical exact (in the sense that there is a precise estimate of the error) solutions to models. QMC achieved some successes like e.g. in providing accurate estimates of correlation energies. Although the methodology presents some intrinsic problems for fermions and the computational time scaling is not favourable, QMC was applied with success to very simple real systems like hydrogen and helium, and starts to be applied to the next Mendeleev table elements.

Another numerical line, mostly followed by chemistry theoreticians, developped from the Hartree-Fock theory. This led to the configuration interaction (CI) theory, a generalization of the Hartree-Fock method to more than one Slater determinant, so to consider more than one electronic configuration and thus account for the *correlation* energy. Indeed, the very mathematical definition of *correlations* is: "all contributions that are missing to the HF approximation". This is exactly in the direction of CI as genuine theory beyond HF. Although one of the most accurate many-body theory, the computational time scaling of CI is extremely unfavourable. CI can be applied only to very small systems, with no more than 10 electrons, which means the very lightest molecules.

Another numerical line took instead the direction to develop *iterative* and *functional* (as opposed to perturbative) approaches to MBQFT. Here the hope was to reformulate the theory in a functional scheme, as originally introduced by Schwinger in elementary particle physics, by individuating a reduced and complete set of quantities for which it could be possible to write a closed set of equations. Starting from the Green's function, the fundamental degree of freedom of MBQFT, one identifies further quantities (the self-energy, the polarizability, ...) as functional of the previously introduced plus new quantities, in the hope that at the end the process closes back. This leads to the Hedin's equations [Hedin 65], a set of 5 integro-differential equations that can be solved iteratively and self-consistently for the 5 quantities, unknown of the problem, starting from a 0-iteration guess for them. Functional approaches allow a new kind of approximations, different from the perturbative scheme, where there can be hope to select the most important contributions. Succesful examples of such approximations are the GW approximation or the Bethe-Salpeter equation (BSE) approach. MBQFT and its approximations will be described in chapter 3.

The most succesful line to address the many-body problem, however, disregarded MBQFT and Green's function theory and rather proposed a further simplification of the problem. This was achieved by replacing the Green's function (and of course the many-body wavefunction) by the simplest electronic density as fundamental degree of freedom of the theory. These are known as density-functional approaches and will be introduced in the next section.

1.3 Density-functional theory (DFT)

Density-functional theory [Hohenberg 64, Kohn 65] is an in principle exact many-body theory to describe ground-state properties such as the total energy, the electronic density, the atomic structure and the lattice parameters. The basic fundamental hyphothesis at the base of the theory is that the ground-state

electronic density $\rho(r)$ of a condensed matter system is a necessary and sufficient quantity to represent all ground-state properties. This is granted by the Hohenberg-Kohn theorem [Hohenberg 64], whose fundamental thesis states that the ground-state electronic density is in an one-to-one correspondence with the external potential $v(r)$, apart from a non-influential constant,

$$\rho(r) \Leftrightarrow v(r) + \text{const.} \tag{1.4}$$

Thank to the Hohenberg-Kohn theorem, all ground-state observables O, and in particular the total energy E, are unique functionals $O[\rho]$ (and $E[\rho]$) of the density. The fundamental degree of freedom of the theory is not any more the complicated many-body wavefunction $\Psi(t, r_1, \ldots, r_N)$, nor the Green's function $G(r_1, t_1, r_2, t_2)$, but the extremely simple ground-state electronic density $\rho(r)$, scalar function of only one space variable. Density-functional theory represents hence a considerable simplification with respect to the direct solution of the many-body Schrödinger equation and also with respect to MBQFT.

The Hohenberg-Kohn theorem provides also a variational principle as a possible scheme to solve the theory: the ground-state density is in correspondence to the global minimum of the total energy functional. Provided we know the total energy as functional dependence on the density[1], we can find the ground-state energy by minimizing the functional,

$$E_0 = \min_{\rho(r)} E[\rho],$$

and in correspondence also the ground-state density $\rho_0(r)$. Any other ground-state quantity can then be calculated, provided we know its functional dependence $O[\rho]$ on the density. The energy density-functional can be decomposed into 4 terms,

$$E[\rho] = T[\rho] + V[\rho] + E_{\mathrm{H}}[\rho] + E'_{\mathrm{xc}}[\rho],$$

where the external potential energy $V[\rho]$ and the Hartree energy $E_{\mathrm{H}}[\rho]$ functionals are

$$V[\rho] = \int dr\, v(r)\rho(r)$$
$$E_{\mathrm{H}}[\rho] = \frac{1}{2}\int dr_1\, dr_2\, w(r_1, r_2)\rho(r_1)\rho(r_2),$$

while the kinetic $T[\rho]$ and the so-called *exchange-correlation* energy $E'_{\mathrm{xc}}[\rho]$ are unknown as functionals and thus representing a problem for the theory. One can at this point develop the theory by resorting to approximations on the unknown terms. Making a *local-density approximation* (LDA) on both the kinetic and exchange-correlation terms gives back the Thomas-Fermi theory, which was not particularly successful. On the other hand, one can develop DFT following Kohn and Sham [Kohn 65]. We introduce a ficticious non-interacting system KS submitted to an effective external potential $v^{\mathrm{KS}}(r)$ under the hyphothesis that its ground-state density $\rho^{\mathrm{KS}}(r)$ is by construction equal to the density of the real system, $\rho^{\mathrm{KS}}(r) = \rho(r)$. For this system we can solve the set of simple

[1]The functional $E[\rho]$ is absolute, independent of the actual condensed matter system.

single-particle equations,

$$\left[-\frac{1}{2}\partial_r^2 + v^{\mathrm{KS}}(r)\right]\phi_i^{\mathrm{KS}}(r) = \epsilon_i^{\mathrm{KS}}\phi_i^{\mathrm{KS}}(r) \tag{1.5}$$

$$\rho(r) = \sum_{i=1}^{N} |\phi_i^{\mathrm{KS}}(r)|^2 \tag{1.6}$$

$$v^{\mathrm{KS}}(r) = v(r) + v_{\mathrm{H}}[\rho](r) + v_{\mathrm{xc}}[\rho](r), \tag{1.7}$$

known as Kohn-Sham equations. Here v_{H} and v_{xc} are defined

$$v_{\mathrm{H}}[\rho](r) = \frac{\delta E_{\mathrm{H}}[\rho]}{\delta\rho(r)} = \int dr'\, w(r,r')\rho(r') \tag{1.8}$$

$$v_{\mathrm{xc}}[\rho](r) = \frac{\delta E_{\mathrm{xc}}[\rho]}{\delta\rho(r)}. \tag{1.9}$$

The set of Kohn-Sham equations must be solved self-consistently, that is for a given initial guess density $\rho(r)$ we calculate the corresponding Kohn-Sham effective potential $v^{\mathrm{KS}}(r)$, Eq. (1.7); then we solve the Schrödinger-like Eq. (1.5) for the Kohn-Sham eigenenergies ϵ_i^{KS} and wavefunctions $\phi_i^{\mathrm{KS}}(r)$; finally we recalculate the next iteration density by Eq. (1.6) and start back the procedure. Once at convergence, we get the ground-state density $\rho_0(r)$ of the KS ficticious system, equal by construction to that one of the real system. Introducing it into the energy functional,

$$E[\rho] = T_{\mathrm{KS}}[\rho] + V[\rho] + E_{\mathrm{H}}[\rho] + E_{\mathrm{xc}}[\rho],$$

we get the ground-state total energy. The Kohn-Sham scheme is a way to better describe the kinetic energy by calculating it at the level of a non-interacting system (the known term $T_{\mathrm{KS}}[\rho]$) and transferring all complications into only one last unknown, which is the exchange-correlation functional $E_{\mathrm{xc}}[\rho]$. The knowledge of this term as a functional of the density is the big unsolved issue of DFT. However, approximations as simple as the local-density approximation (LDA) [Kohn 65], and better on, the generalized gradient approximation (GGA), have demonstrated to work well on the large majority, say 99% of condensed matter systems. Typical *ab initio* DFT errors on ground-state total energies, atomic structures or lattice parameters, are within a few per cent off the experiment, depending on the approximation. For this reason and for its inherent simplicity, density-functional theory is one of the most succesful physics theories ever formulated [Redner 05].

Owing to its success on ground-state properties, DFT in the Kohn-Sham scheme is commonly used to describe not only the ground-state density and energy, but also electronic excitations and spectroscopy. In practice the electronic structure of the ficticious non-interacting Kohn-Sham system, which in principle has no physical meaning, is used to describe the true quasiparticle electronic structure of the real system. *This procedure has no physical foundation.* Kohn-Sham DFT is not an in principle exact framework for electronic excitations and spectroscopy. KS results can be good for some systems and some excitations, but there is no guarantee that this is sistematic. For instance, it turns out that DFT in the LDA or the GGA approximations sistematically underestimate the

band gap by a 40%. One might hope that the failure of DFT in describing electronic excitations is due to a failure of the exchange-correlation approximation and try to go beyond LDA or GGA, toward a better approximation. But even the true, exact exchange-correlation potential is not supposed to reproduce excitations. And we demonstrated [Gatti 07c] that an effective theory with a static and local potential $v(r)$, like the effective Kohn-Sham theory, has not enough degrees of freedom to be able to in principle describe e.g. the band gap of even a simple model system like the jellium with gap (Callaway model). An effective theory that can in principle access the band gap must have a potential that is either non-local or dynamical, which is not the case of the ordinary Kohn-Sham exchange-correlation potential.

In order to describe electronic excitations, two ways can be followed at this point: In the first, one keeps a DFT Kohn-Sham scheme and ask for an approximation to the exchange-correlation potential that tries to do its best in describing the true quasiparticle electronic structure and excitations. That is, we search for the best static and local *phenomenological* approximation to the true non-local and dynamic self-energy, so that it can be put in the form of an effective Kohn-Sham potential and used within a Kohn-Sham scheme not only to calculate ground-state properties, but also the quasiparticle electronic structure. Along this way one is satisfied with an electronic structure that can be even a rough approximation to the true quasiparticle structure, but the advantage is that the calculation is as simple as a DFT calculation. This is a way we followed effectively during my PhD thesis work [Olevano 99b, Olevano 00]. We tried to parametrize the exchange-correlation potential in the form of an ordinary LDA approximation plus a Slater exchange term. Then we adjusted the free phenomenological parameters so that the theory could reproduce the band gap of semiconducting and insulating system with the least error with respect to the in principle correct many-body self-energy formalism, using the best approximation at disposal, i.e. GW. That work concluded that the LDA approximation is the best static and local approximation for the GW self-energy. But we did not exclude that there could exist more complicated parametrizations than ours, introducing much more free parameters, so to improve with respect to LDA.

The second way is to go beyond ordinary DFT. One possibility is time-dependent density-functional theory (TDDFT), an extension of static DFT to time-dependent phenomena. That is a way we started to explore during my PhD thesis. In particular, we showed [Olevano 99b, Olevano 99a] how good TDDFT is, even in the most elementary approximations like random-phase approximation (RPA) with local-field effects (LFE) and adiabatic local-density approximation (ALDA or TDLDA), in reproducing and predicting with a very good, even quantitative, agreement both electron-energy loss (EELS) and inelastic X-ray scattering spectroscopy (IXSS). On the other hands, we demonstrated like simple approximations to the exchange-correlation functional, like RPA, TDLDA or even jellium based non-local approximations (NLDA), can at best reproduce optical spectra only qualitatively. In particular, in semiconductors and insulators we found a sistematic red shift of spectra together with an underestimation of the lowest energy part. The objective to find better approximations in order to improve the performances of TDDFT also for optical spectroscopy, was the subject of our work in the years later and the topic of the next section on TDDFT.

Chapter 2

TDDFT: from EELS to optical spectra

In this chapter we will draw the fundamentals of TDDFT theory, from the Runge-Gross theorem to the Kohn-Sham scheme, focusing in particular to linear-response TDDFT. The `DP` code is an implementation of LR-TDDFT in frequency-reciprocal space and plane-waves. We will then introduce the basic RPA and ALDA (or TDLDA) approximations and see how good they are on EELS, IXSS or CIXS spectra at the example of bulk silicon. We will show the effect on spectra of crystal local-fields (LF), whose importance grows in systems presenting strong inhomogeneities in the electronic density. In particular, local-fields are strongly affected by atomic structure reduced-dimensionality confinement effects. Although simple, LF effects have been our true "battle horse" all along these years. The last sections will present our contributions to the development of better TDDFT exchange-correlation kernel approximations, in order to describe optical spectra as measured by ellipsometry. We will first present the *long-range contribution* (LRC) kernel (also known as α/q^2 kernel) and the so-called *Nanoquanta* kernel. We will show how good they are on optical absorption and finally discuss the still open points of the theory.

In according to the rules stated for a HDR manuscript, we indicate here that the development of TDDFT in the RPA (with or without LF effects), TDLDA (plus some other non-local kernels) and the implementation of the `DP` code, have been carried out during my PhD thesis work [Olevano 99b]. This was already sufficient to have good results on EELS, IXSS and CIXS spectra. However all the work on new approximations, in order to make TDDFT work also on optical spectra, has been carried out in the years after. The work on the α/q^2 kernel already started during the PhD in Rome, but the right recipe to make it work was found only later, in Palaiseau [Reining 02]. The work on the Nanoquanta kernel [Sottile 03b] was carried out by F. Sottile and his PhD thesis' work supervised by L. Reining with also a non-official supervision by myself.

2.1 The Runge-Gross theorem

In order to go beyond ground-state properties but always staying in the spirit of density-functional like theories, one can try to put on the same footing the external static potential (due to the ions) $v(r)$ and the external perturbation which excites the system $\delta v(r,t)$. Going on along this way, one can do a density-functional theory considering as external potential the sum of the two terms,

$$v(r,t) = v(r) + \delta v(r,t). \tag{2.1}$$

The extra complication is that the external perturbation, for example an incident electromagnetic wave or an electron beam switched on at an initial time t_0, is in general represented by a time-dependent external potential $\delta v(r,t)$. And the Hohenberg-Kohn theorem holds only for static external potentials. DFT does not apply to time-dependent external potentials and for this reason cannot describe excitations.

The solution to this issue is represented by the Runge-Gross theorem [Runge 84] which extends the Hohenberg-Kohn theorem to the time-dependent case. The Runge-Gross theorem states that the time-dependent electronic density is in a one-to-one correspondence with the external (time-dependent) potential, up to an uninfluential merely time-dependent constant,

$$\rho(r,t) \Leftrightarrow v(r,t) + \text{const}(t). \tag{2.2}$$

It becomes hence possible to build a time-dependent density-functional theory following the scheme of DFT. In analogy with DFT, in TDDFT any observable $O(t)$ is a unique functional $O[\rho](t)$ of the time-dependent density $\rho(r,t)$. There are however some differences and some *caveats*. The first one is that any observable is in reality a unique functional $O[\rho, \Psi_0](t)$ of the density *and* of the initial state $\Psi_0 = \Psi(t_0)$. We reintroduce the complication to deal with many-body wavefunctions, although only to fix boundary conditions. To overcome this problem, we can always assume that the initial state is the ground-state, the usual situation for common problems, and address this issue by static DFT.

The second problem is that the Runge-Gross theorem has been demonstrated for a much more restricted domain of validity than the Hohenberg-Kohn theorem. There does not exist a general proof of the Rnuge-Gross theorem for arbitrary time-dependent potentials $v(r,t)$, although it has been demonstrated for several classes of different potentials, so that one may hope that the theorem is more general than actually demonstrated. In particular, the original Runge-Gross demonstration relies on the hypothesis that the external potential $v(r,t)$ is Taylor expandable around the initial time t_0. This excludes step-like switch-on $v(r,t) = v(r) + \delta v\, \theta(t - t_0)$ potentials that are non analytical in t_0. The external perturbation should be switched on gently, for example adiabatically. But this implies that the initial state at t_0 cannot be the ground-state, since to build the ground-state we need that the external perturbation be switched off $\delta v(r,t) = 0$ for sufficient long times $t < t_0$ before t_0. And so we run again into the first problem. All these are questions of principle. We can however go on and assume that for example the domain of validity of the Runge-Gross theorem is larger than provided in the original demonstration, so that it can deal also with non-analytical time-dependent external potentials.

Going on with the analogies and the differences between DFT and TDDFT, the place that in DFT is assumed by the energy functional $E[\rho] = \langle\Psi|\hat{H}|\Psi\rangle$, is in the case of TDDFT taken by the action,

$$A[\rho] = \int_{t_0}^{t_1} dt \left\langle \Psi(t) \middle| i\partial_t - \hat{H} \middle| \Psi(t) \right\rangle.$$

Like in DFT where there exists a variational principle on the total energy, in TDDFT the stationary points $\delta A[\rho]/\delta\rho(r,t) = 0$ of the action provide the exact time-dependent density $\rho(r,t)$ of the system.

We can introduce a Kohn-Sham system and solve the theory following a Kohn-Sham scheme also in TDDFT. With respect to static DFT, the Kohn-Sham equation will be a time-dependent Schrödinger-like equation and the Kohn-Sham potential will contain a term related to the exchange-correlation action $A_{\rm xc}[\rho]$, instead of the exchange-correlation energy. Kohn-Sham equations in TDDFT read:

$$i\partial_t \phi_i^{\rm KS}(r,t) = \left[-\frac{1}{2}\partial_r^2 + v^{\rm KS}(r,t)\right] \phi_i^{\rm KS}(r,t) \tag{2.3}$$

$$\rho(r,t) = \sum_i |\phi_i^{\rm KS}(r,t)|^2 \tag{2.4}$$

$$v^{\rm KS}(r,t) = v(r,t) + v_{\rm H}[\rho](r,t) + \frac{\delta A_{\rm xc}[\rho]}{\delta\rho(r,t)}. \tag{2.5}$$

When following the Kohn-Sham scheme, we run into further *caveats*. Indeed, the exchange-correlation action functional $A_{\rm xc}[\rho]$ is defined only for v-representable densities, i.e. it is undefined for densities $\rho(r,t)$ which do not correspond to some potential $v(r,t)$. This leads to a problem when, in order to search for stationary points, we require variations $\delta A_{\rm xc}[\rho]$ with respect to arbitrary density variations $\delta\rho$. It is the so called v-representability problem which is however present also in DFT and has already been solved [Levy 82].

There is finally a last problem related to the so called causality-symmetry paradox, which also has been already solved [van Leeuwen 98] by requiring the time t to be defined on the Keldysh contour (Fig. 4.1) instead of the real axis.

2.2 TDDFT in linear response

Most of the previous problems are however shortcut when working in the linear response regime [Gross 85]. Suppose that we can split the time-dependent external potential into a purely static term (to be identified, as usual, to the potential generated by the positive ions) and a time-dependent perturbation term, as in Eq. (2.1),

$$v(r,t) = v(r) + \delta v(r,t),$$

and suppose that the time-dependent perturbation term is much smaller than the static term,

$$\delta v(r,t) \ll v(r), \tag{2.6}$$

then the theory can be factorized into an ordinary static density-functional theory plus a linear response theory to the small time-dependent perturbation. In this case the Hohenberg-Kohn and the Runge-Gross theorems together state

that the linear response time-dependent variation to the density is one-to-one with the time-dependent perturbation to the external potential,

$$\delta\rho(r,t) \Leftrightarrow \delta v(r,t).$$

The condition Eq. (2.6) is usually verified when considering normal situations that refer to condensed matter systems submitted to slight excitation. This is the case in optical spectroscopy using ordinary light, energy-loss spectroscopy or X-ray spectroscopies. On the other hand, for spectroscopies implying strong electromagnetic fields, intense lasers and so on, condition Eq. (2.6) does not hold any more and the situation cannot be described by linear-response TDDFT.

A linear-response TDDFT (LR-TDDFT) calculation consists in two steps: starting from the static ionic external potential $v(r)$, we perform an ordinary static DFT calculation of the Kohn-Sham energies ϵ_i^{KS} and wavefunctions $\phi_i^{\mathrm{KS}}(r)$ and hence of the ground-state electronic density $\rho(r)$; then we do a linear-response TDDFT calculation of the density variation $\delta\rho(r,t)$ corresponding to the external time-dependent perturbation $\delta v(r,t)$. From $\delta\rho(r,t)$ we can then calculate the *polarizability* χ of the system which is defined as the linear response proportionality coefficient $\delta\rho = \chi\delta v$ of the density with respect to the external potential,

$$\delta\rho(x_1) = \int dx_2\, \chi(x_1,x_2)\delta v(x_2), \tag{2.7}$$

where we have used the notation to indicate with x the space and time variables, $x = \{r,t\}$, eventually including also the spin index, $x = \{r,t,\xi\}$. In the next, when clear from the context, we will simplify the notation omitting convolution products $\int dx$ as in Eq. (2.7).

2.3 Kohn-Sham scheme in LR-TDDFT

It is possible to follow a Kohn-Sham scheme also in linear-response TDDFT. The first step is to introduce a ficticious non-interacting Kohn-Sham system KS under the hypothesis that its density response $\delta\rho^{\mathrm{KS}}$ is equal to the density response of the real system $\delta\rho = \delta\rho^{\mathrm{KS}}$ when answering to an effective (Kohn-Sham) external perturbation δv^{KS},

$$\delta v^{\mathrm{KS}}(x) = \delta v(x) + \delta v_{\mathrm{H}}(x) + \delta v_{\mathrm{xc}}(x), \tag{2.8}$$

where

$$\delta v_{\mathrm{H}}(x_1) = \int dx_2\, w(x_1,x_2)\delta\rho(x_2), \tag{2.9}$$

$$\delta v_{\mathrm{xc}}(x_1) = \int dx_2\, f_{\mathrm{xc}}[\rho](x_1,x_2)\delta\rho(x_2), \tag{2.10}$$

$$f_{\mathrm{xc}}[\rho](x_1,x_2) = \frac{\delta v_{\mathrm{xc}}[\rho](x_1)}{\delta\rho(x_2)}. \tag{2.11}$$

$w(x_1,x_2) = \delta(t_1,t_2)1/|r_2 - r_1|$ is the Coulombian and $f_{\mathrm{xc}}[\rho](x_1,x_2)$ is the so called exchange-correlation kernel, defined as the second density-functional derivative of the exchange-correlation energy E_{xc} with respect to the density (the first derivative of the exchange-correlation potential v_{xc}). f_{xc} is the fundamental quantity in linear-response TDDFT and also the big unknown.

For the ficticious KS independent particle system we can introduce the corresponding *Kohn-Sham polarizability* $\chi^{\rm KS}$ as

$$\delta\rho(x_1) = \int dx_2\, \chi^{\rm KS}(x_1, x_2)\delta v^{\rm KS}(x_2), \tag{2.12}$$

that is, the polarizability of the independent-particle system which responds to the external perturbation $\delta v^{\rm KS}$ by the density variation $\delta\rho$. By applying perturbation theory to the Kohn-Sham equation (2.3), it can be shown that the Kohn-Sham polarizability is provided by the analytic expression (in r-ω space)

$$\chi^{\rm KS}(r_1, r_2, \omega) = \sum_{i,j\neq i} (f_i^{\rm KS} - f_j^{\rm KS}) \frac{\phi_i^{\rm KS}(r_1)\phi_j^{\rm KS\,*}(r_1)\phi_j^{\rm KS}(r_2)\phi_i^{\rm KS\,*}(r_2)}{\epsilon_i^{\rm KS} - \epsilon_j^{\rm KS} - \omega - i\eta}, \tag{2.13}$$

(the $f^{\rm KS}$ are occupation numbers) known as Adler-Wiser expression [Adler 62, Wiser 63]. The Kohn-Sham polarizability can hence be calculated once we have solved the static DFT problem and we know the DFT Kohn-Sham energies $\epsilon_i^{\rm KS}$ and wavefunctions $\phi_i^{\rm KS}(r)$. By combining Eqs. (2.7), (2.12) and (2.8), we can express the polarizability χ of the real system in a Dyson-like form,

$$\chi = \chi^{\rm KS} + \chi^{\rm KS}(w + f_{\rm xc})\chi, \tag{2.14}$$

or also in an explicit form,

$$\chi = (1 - \chi^{\rm KS}w - \chi^{\rm KS}f_{\rm xc})^{-1}\chi^{\rm KS}, \tag{2.15}$$

in terms of the Kohn-Sham polarizability $\chi^{\rm KS}$ and of the unknown exchange-correlation kernel $f_{\rm xc}$. So, once we have an expression for the kernel, it is relatively easy to calculate in LR-TDDFT the polarizability χ and hence spectra.

2.4 The exchange-correlation kernel $f_{\rm xc}$

The most common approximations for the exchange-correlation kernel are the *random-phase approximation* (RPA) and the *adiabatic local-density approximation* (indicated as ALDA or also TDLDA). In the RPA approximation the exchange-correlation kernel is set to zero, $f_{\rm xc} = 0$, and exchange-correlation effects are neglected. This is not such a crude approximation as one may think. Indeed, exchange-correlation effects are neglected only in the linear-response to the external perturbation. Not in the previous static DFT calculation, where they are taken into account by choosing an appropriate exchange-correlation potential $v_{\rm xc}$, in LDA or GGA for example. In the next we will see examples of the validity of this approximation.

In the adiabatic local-density approximation, the kernel is taken to be

$$f_{\rm xc}^{\rm ALDA}(x_1, x_2) = \frac{\delta v_{\rm xc}^{\rm LDA}[\rho](x_1)}{\delta\rho(x_2)} = \delta(x_1, x_2) f_{\rm xc}^{\rm HEG}(\rho(r)), \tag{2.16}$$

which is a local and and ω-independent static (instantaneous) expression. As we will show, TDLDA is a good approximation to calculate EELS or IXSS and even CIXS spectra. RPA and TDLDA are however unsatisfactory for optical spectra in semiconductors and insulators, i.e. spectra where electron-hole (e-h) interaction effects, giving rise to bound excitons or excitonic effects, are

important. To provide new good approximations for the exchange-correlation kernel beyond ALDA and to make TDDFT work also on optical properties, was the motivation of the last 10 years research efforts. This will be presented in the last part of this chapter.

2.5 Dielectric function and spectra

From the polarizability we can calculate the *microscopic dielectric function* $\varepsilon(x_1, x_2)$,

$$\varepsilon^{-1} = 1 + w\chi. \tag{2.17}$$

Observable quantities and spectra are related to the *macroscopic dielectric function* ε_{M} obtained from the microscopic ε by spatially averaging over a distance large enough with respect to the microscopic structure of the system, for example in solids an elementary cell,

$$\varepsilon_{\mathrm{M}}(r, r', \omega) = \overline{\varepsilon(r, r', \omega)}. \tag{2.18}$$

It can be shown that in reciprocal space the operation of averaging corresponds to the expression

$$\varepsilon_{\mathrm{M}}(q, \omega) = \frac{1}{\varepsilon^{-1}_{G=0,G'=0}(q, \omega)}, \tag{2.19}$$

that is, the macroscopic ε_{M} is equivalent to the inverse of the $G = G' = 0$ element (G and G' reciprocal-space vectors) of the reciprocal-space *inverse* microscopic dielectric matrix ε^{-1}. This does not correspond to the $G = G' = 0$ element of the *direct* microscopic dielectric matrix ε,

$$\varepsilon^{\mathrm{NLF}}_{\mathrm{M}}(q, \omega) = \varepsilon_{G=0,G'=0}(q, \omega), \tag{2.20}$$

in all the cases where the microscopic dielectric matrix contains off-diagonal terms. The expression Eq. (2.20) is an *approximation* (NLF) to the exact macroscopic dielectric function. By this approximation the so-called crystal *local-field* effects are neglected (no local-field effects, NLF). These effects are absent in the homogeneous electron gas, they are marginal in weakly inhomogeneous systems (e.g silicon), but become important in systems presenting strong inhomogeneities in the electronic density. In particular, local-field effects are critical in reduced dimensionality systems (2D surfaces/graphene, 1D nanotubes/wires, 0D clusters etc.).

The macroscopic dielectric function is the key quantity to calculate observables and spectra. For example the *dielectric constant* is given by

$$\varepsilon_\infty = \lim_{q \to 0} \varepsilon_{\mathrm{M}}(q, \omega = 0). \tag{2.21}$$

The ordinary *optical absorption*, as measured e.g. in ellipsometry, is directly related to the imaginary part of the macroscopic dielectric function,

$$\mathrm{ABS}(\omega) = \Im\varepsilon_{\mathrm{M}}(q \to 0, \omega). \tag{2.22}$$

Finally, the *energy-loss function*, as measured in EELS or IXSS, is related to minus the imaginary part of the inverse macroscopic dielectric function,

$$\mathrm{ELF}(q, \omega) = -\Im\varepsilon^{-1}_{\mathrm{M}}(q, \omega). \tag{2.23}$$

2.6 The DP code

The equations presented in the previous sections have been implemented during my PhD thesis work in the DP code [Olevano 98]. DP is a linear-response TDDFT code on a plane-waves basis set working in frequency-reciprocal space, although some quantities are calculated in frequency-real space. The code allows to calculate dielectric and optical spectra such as optical absorption, reflectivity, refraction indices, EELS, IXSS, CIXS spectra. It uses periodic boundary conditions and works both on bulk 3D systems and also, by using supercells containing vacuum, on 2D surfaces, 1D nanotubes/wires and 0D clusters and molecules. The systems can be insulating or metallic. It implements several approximations for the exchange-correlation kernel and local-field effects can be switched on and off.

The DP code relies on a previous DFT calculation of the KS energies and wavefunctions provided by another PW code, for example ABINIT [Gonze 09]. The first task is to back Fourier transform the KS wavefunctions $\phi_i^{\mathrm{KS}}(G) \rightarrow \phi_i^{\mathrm{KS}}(r)$ from reciprocal to real space. Then DP calculates in real space the optical matrix elements $\rho_{ij}^{\mathrm{KS}}(r) = \phi_i^{\mathrm{KS}\,*}(r)\phi_j^{\mathrm{KS}}(r)$, which are Fourier transformed $\rho_{ij}^{\mathrm{KS}}(r) \rightarrow \rho_{ij}^{\mathrm{KS}}(G)$ to reciprocal space. The next step is to calculate the Kohn-Sham polarizability,

$$\chi^{\mathrm{KS}}_{G_1G_2}(q,\omega) = \sum_{i,j\neq i} (f_i^{\mathrm{KS}} - f_j^{\mathrm{KS}}) \frac{\rho_{ij}^{\mathrm{KS}}(G_1,q)\rho_{ij}^{\mathrm{KS}\,*}(G_2,q)}{\epsilon_i^{\mathrm{KS}} - \epsilon_j^{\mathrm{KS}} - \omega - i\eta}. \tag{2.24}$$

At this point the RPA dielectric function and spectra in the NLF approximation are already available via $\varepsilon_{\mathrm{M}}^{\text{RPA-NLF}}(q,\omega) = 1 - w\chi_{00}^{\mathrm{KS}}(q,\omega)$. For approximations beyond, DP first calculates the polarizability χ by Eq. (2.15). The ALDA exchange-correlation f_{xc} is calculated in real space and then Fourier transformed in reciprocal space. At the end, DP calculates the dielectric function ε (Eq. (2.17)) and finally the observable macroscopic dielectric function $\varepsilon_{\mathrm{M}}(q,\omega)$ (Eq. (2.19)) including local-field effects. $\varepsilon_{\mathrm{M}}(q,\omega)$ is provided in an output file both in the real and in the imaginary part as a function of ω (the BZ vector q is fixed and specified as input parameter to the DP code). The most time consuming steps are the calculation of χ^{KS}, where Fourier transforms are carried out using FFT (scaling $N \log N$ instead of N^2), and the matrix inversion to calculate χ (Eq. (2.15)), which is however replaced by the resolution of a linear system of equations (scaling N^2 instead of N^3).

2.7 RPA and TDLDA approximations

We will now show examples of typical TDDFT results using the RPA and TDLDA approximations on both the optical absorption and the energy-loss spectra of a prototypical system like bulk silicon. Fig. 2.1 presents the experimental imaginary part of the macroscopic dielectric function $\Im\varepsilon(\omega)$ (red dots) directly related to the optical absorption as measured by e.g. the ellipsometry experiment of Ref. [Lautenschlager 87]. Then we show a DP code calculation [Olevano 99b] of the RPA with and without LF effects and TDLDA spectra. We remark "some" qualitative agreement of TDDFT with the experiment. Indeed, we observe in the experiment 3 peeks, at 3.5, 4.3 and 5.3 eV, which are more

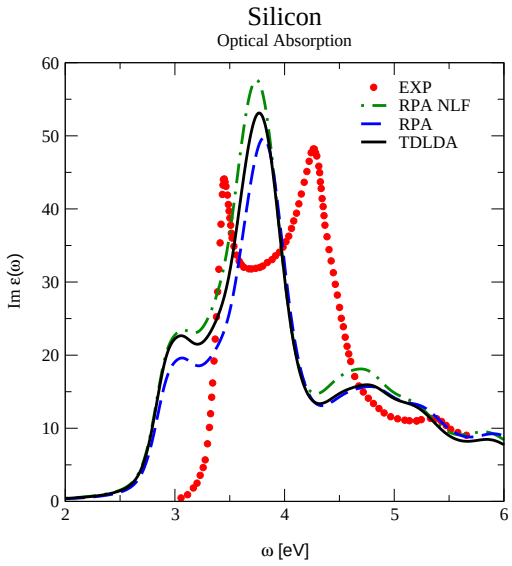

Figure 2.1: Optical absorption in silicon (reproducing Fig. 2 of Ref. [Olevano 99a]). Imaginary part of the macroscopic dielectric function in the RPA without (NLF, green dot-dashed line) and with local-field effects (blue dashed line), TDLDA (black continuous line), ellipsometry experiment (red dots from Ref. [Lautenschlager 87]).

or less reproduced by 3 structures in the theory, whether in RPA or TDLDA approximation. Local-field effects seem to have the same weight as exchange-correlation effects on the result (compare RPA curves with and without (NLF) local-field effects). We also remark that there is no improvement in passing from RPA to TDLDA approximation. The agreement with the experiment is unsatisfactory for 2 reasons:

1. The TDLDA (or RPA) optical onset appears to be red-shifted by ~ 0.6 eV with respect to the experiment. The whole spectrum (not only the onset, but also the 3 structures) seems rigidly red-shifted with respect to the experiment by the same amount.

2. The height of the first lowest energy peak seems underestimated by the theory with respect to the experiment. Both in RPA and TDLDA this peak appears like a shoulder of the main peak, while in the experiment it is almost the same height. Nevertheless, we remark some agreement between theory and experiment on the height of the second and third highest energy peaks.

The cause of the first problem seems quite easy to understand. Indeed, 0.6 eV is exactly the band gap underestimation of the DFT-LDA Kohn-Sham electronic structure with respect to the true quasiparticle electronic structure in silicon. A quasiparticle self-energy calculation as in the GW approximation [Hybertsen 85, Godby 87] takes into account in a satisfactory way correlation electron-electron (e-e) interaction effects and corrects the DFT band gap un-

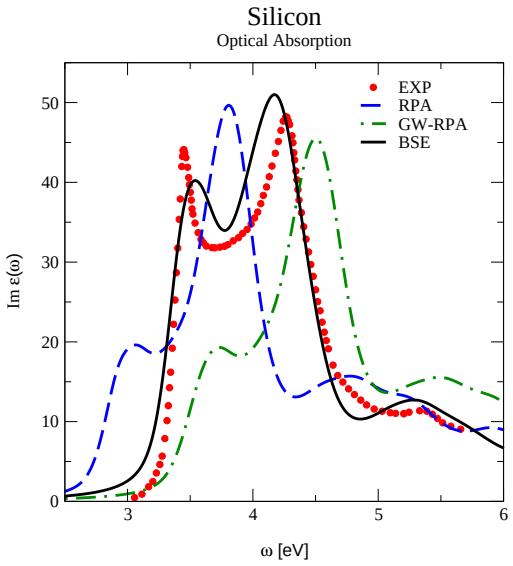

Figure 2.2: Optical absorption in silicon (reproducing Fig. 1 of Ref. [Albrecht 98]). Imaginary part of the macroscopic dielectric function in the RPA (blue dashed line), GW-RPA (green dot-dashed line), Bethe-Salpeter equation approach (BSE, black continuous line), ellipsometry experiment (red dots from Ref. [Lautenschlager 87]).

derestimation. A GW-RPA spectrum (calculated using an RPA approximation on top of a GW electronic structure) will hence result blue-shifted with respect to the KS-RPA spectrum by a 0.6 eV (see the GW-RPA curve in Fig. 2.2). The position of the optical onset, and somehow also of the other structures, are now more in agreement with the experiment. The remaining disagreements, in particular the underestimation of the first low-energy peak, have hence to be ascribed to electron-hole (e-h) interaction effects which are missing in the GW-RPA approximation. e-h interaction effects give rise to bound excitons in insulators. In materials where the screening is a little bit larger like in semiconductors, they give rise to so-called excitonic effects which manifest with a strengthening of the lowest energy part of optical absorption spectra. e-h interaction excitonic effects are correctly reproduced when going beyond the GW-RPA approximation by introducing vertex corrections via the *ab initio* Bethe-Salpeter equation (BSE) approach. This is demonstrated by a BSE calculation [Albrecht 98] of the optical absorption as reported in Fig. 2.2. The BSE curve corrects the underestimation of the first peak, as well as the small residual blue-shift of the spectrum, and is now in good agreement with the experiment. The conclusion is that, although TDDFT is an in principle exact theory to predict neutral excitations and spectra, the ALDA approximation on the xc kernel fails to reproduce optical spectra. The true unknown exact kernel should describe both e-e and e-h effects, at the same time, while the ALDA kernel does not.

The conclusions are however completely different when considering energy-loss spectra (EELS). Fig. 2.3 shows the EELS experimental spectrum (red dots measured at $q \sim 0$ by Ref. [Stiebling 78]). The spectrum presents a single peak

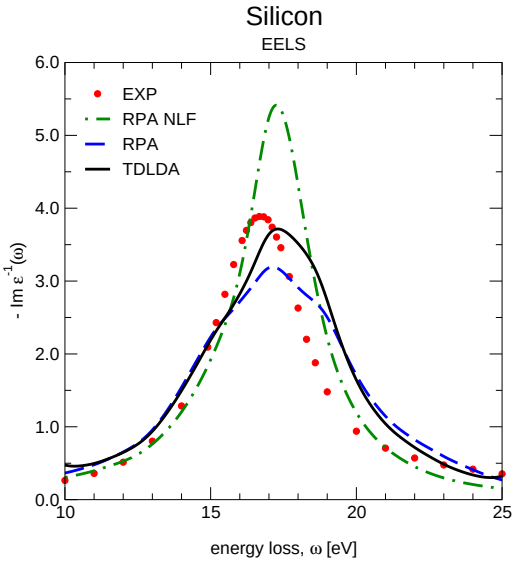

Figure 2.3: Energy-loss spectra (EELS) in silicon (reproducing Fig. 3 of Ref. [Olevano 99a]). Energy-loss function at $q \simeq 0$ in the RPA without (NLF, green dot-dashed line) and with local-field effects (blue dashed line), TDLDA (black continuous line), EELS experiment (red dots from Ref. [Stiebling 78]).

at $\sim$ 16.7 eV corresponding to the plasmon resonance collective excitation of bulk silicon. We then show the energy-loss function calculated [Olevano 99b] by the `DP` code in the RPA NLF (without local-field effects), the RPA and TDLDA approximations using the `DP` code. Here we remark that the overall agreement of TDLDA with the experiment is very good. Both the position and the height of the plasmon resonance are correctly reproduced by the TDLDA approximation. Also we can conclude that the RPA result at $q \sim 0$ is not such bad and at least qualitatively in agreement. This surprising result can be explained when looking at Fig. 2.4 where we present the result of a Bethe-Salpeter equation approach calculation [Olevano 01] on EELS. Here we remark that when introducing *e-e* interaction effects by passing from RPA on top of a KS to RPA on top of a GW electronic structure (GW-RPA curve) the result surprisingly worsens and shifts away from the experiment toward the highest energies. It is only thank to the introduction of *e-h* interaction effects on top of the GW *e-e* interaction effects by resolution of the Bethe-Salpeter equation (BSE curve) that the result shifts back again and recovers a good agreement with the experiment. Thus it turns out that on EELS *e-e* and *e-h* interaction effects compensate each other, and a low level of approximation as RPA on top of KS is in better agreement with the experiment than GW-RPA. TDLDA just adds those small exchange-correlation effects necessary to improve upon RPA.

This improvement upon RPA becomes more and more appreciable when the transferred momentum q becomes larger, as it is possible to measure by IXSS spectroscopy. In Fig. 2.5, we show the dynamic structure factor (directly related to the energy-loss function) at $q = 1.25$ a.u. along the [111] direction for silicon. The red curve is the IXSS experiment of Ref. [Weissker 06] carried out at the

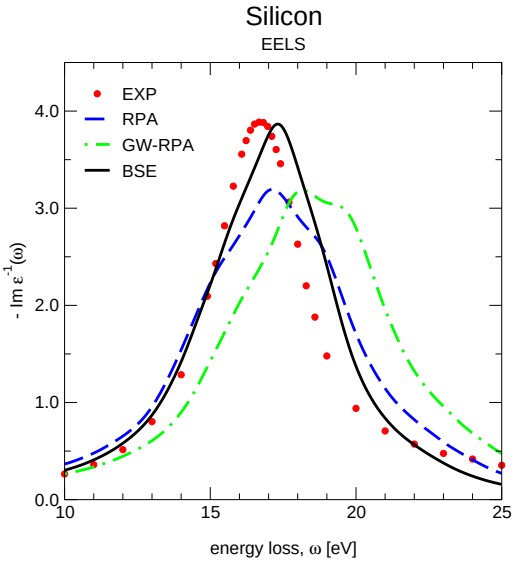

Figure 2.4: Energy-loss spectra (EELS) in silicon (reproducing Fig. 2 of Ref. [Olevano 01]). Energy-loss function in the RPA (blue dashed line), GW-RPA (green dot-dashed line) Bethe-Salpeter approach (BSE black continuous line), EELS experiment (red dots from Ref. [Stiebling 78]).

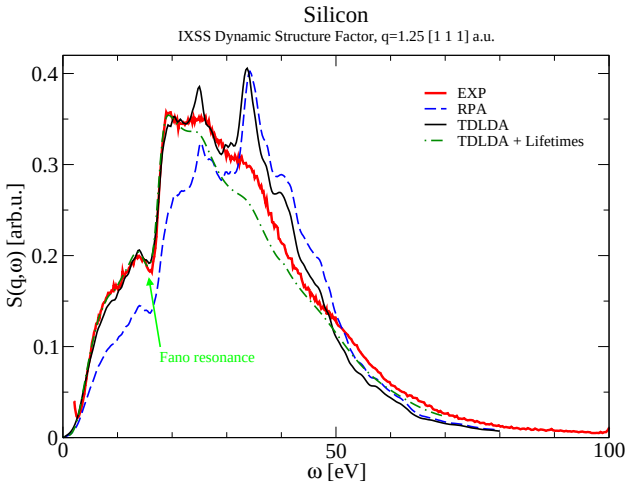

Figure 2.5: Inelastic X-ray scattering spectra (IXSS) in silicon (see Fig. 4 of Ref. [Olevano 99a] and Fig. 1 of Ref. [Weissker 06]). Dyamic structure factor at $q = 1.25$ a.u. along [111] in the RPA (blue dashed line) TDLDA (black continuous line) and IXSS experiment (red dots from Ref. [Sturm 92, Weissker 06]).

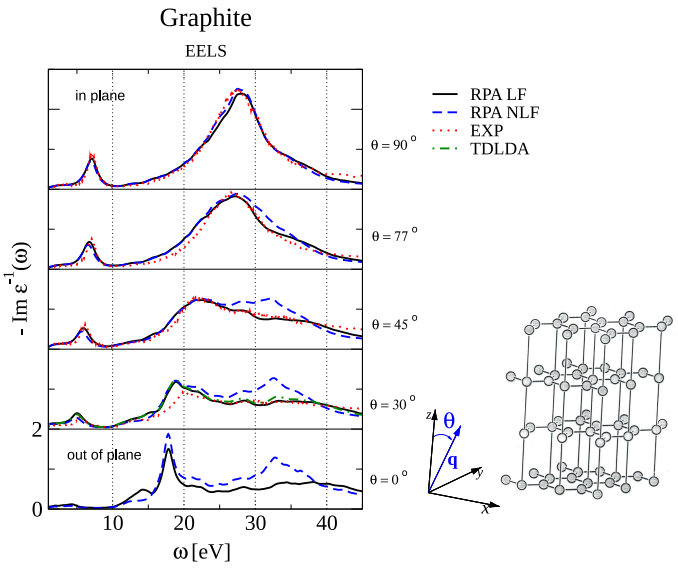

Figure 2.6: EELS spectra of graphite (from Ref. [Marinopoulos 02, Marinopoulos 04]) for small q transferred momentum at several directions, from in plane (top) to out-of-plane (bottom). Red dots: experiment; blue dashed line: RPA without LF effects; black solide line: RPA with LF; green dot-dashed line: TDLDA.

ESRF synchrotron which reproduces an older experiment [Sturm 92]. We then show the RPA and TDLDA results calculated [Olevano 99b, Weissker 06] using the `DP` code. It turns out that TDLDA continues to be in very good agreement with the experiment, especially at the lowest energies. TDLDA is even able to reproduce the structure at 17 eV which is a Fano resonance with its typical asymmetric shape. The Fano resonance here is due to the interaction of a discrete excitation (the plasmon at ∼17 eV in Si) and the continuum of e-h excitations. The oscillations at higher energies have been ascribed to lifetime effects and corrected in Ref. [Weissker 06] by introducing a Fermi-liquid quadratic imaginary part to the energies. At the highest q, RPA turns out to be more and more faraway from TDLDA and in worst agreement with the experiment.

2.8 Atomic structure and local-field effects

We conclude this section by showing the importance of local-field effects in systems presenting strong density inhomogeneities especially due to the atomic structure. In particular in systems presenting a *reduced dimensionality atomic structure*[1]. Local-field effects are particularly sensitive to reductions in the dimensionality of the atomic structure and thus are particularly strong e.g. in 1D nanotubes or nanowires. To show this critical point we take the example of

[1]This is not the same as *reduced dimensionality electronic structure*. Here we are talking about systems where the atomic structure lives on a 2D manifold or less, 1D, 0D. Electrons are free to wander in all the other dimensions.

graphite [Marinopoulos 02, Marinopoulos 04], a system of intermediate 3D/2D character: it is in fact a 3D bulk solid but its carbon atoms are arranged in 2D flat planes of graphene, weakly bounded and stacked one over the other. As a consequence of this particular atomic structure, the system looks homogeneous in a xy-direction, while it appears inhomogeneous along the z-direction. This is immediately appreciable in EELS when varying the direction of the transferred momentum q (Fig 2.6), from in plane (top) to out-of-plane (bottom). The red dots are the experiment, done for small q with the indicated angle θ with respect to z. The important point to remark is how the RPA with and without LF effects practically coincide when in plane (homogeneous system), while they start to differ when sampling out-of-plane, reaching the maximum when along z (inhomogeneous system). Of course, it is always the curve with LF effects included which is in good agreement with the experiment. For this small q, xc effects are small. Thus along the direction where the difference between the theoretical results with and without LF effects is large, the system presents an inhomogeneity which is a direct consequence of its particular atomic structure along that direction. When studying truly atomic structure reduced dimensionality systems like 2D graphene or 1D nanotubes, LF effects are very large along the direction perpendicular to the 2D plane or the 1D nanotubeaxis. Along these directions LF gives rise to so-called depolarization effects, strong suppressions of the imaginary part of the dielectric function that can extend even for several eV.

All these conclusions have been confirmed by plenty of other calculations on very different systems all along these years by us as well as many other authors. The main conclusion is that the ALDA xc kernel is a very good approximation to predict energy-loss spectra, but is a poor approximation to calculate optical spectra in insulators and semiconductors. This is a puzzle to be solved in order to devise better approximations and improve over ALDA on optical spectra. Local-field (LF) effects are normally equally important as exchange-correlation, and they become fundamental in systems with reduced dimensionality atomic structure.

2.9 Long-range contribution (LRC) α/q^2 kernel

An important original contribution we think to have provided to TDDFT is the introduction of a new xc kernel, we have called long-range contribution (LRC) only, or also α/q^2 kernel for its mathematical shape in reciprocal space,

$$f_{\rm xc}^{\rm LRC}(q) = \frac{\alpha}{q^2}, \tag{2.25}$$

where α was regarded at that time as a material dependent adjustable parameter. From the real space expression of this kernel,

$$f_{\rm xc}^{\rm LRC}(r, r') = \frac{\alpha}{4\pi|r - r'|}, \tag{2.26}$$

it can be seen that this kernel contains an ultra non-local, i.e. a long-range Coulumb-like contribution that represents the important difference with respect to the ALDA kernel Eq. (2.16) which is instead local.

We now explain why an LRC kernel can do the right job. We have already seen (Fig. 2.1) that for optical properties a local kernel like ALDA has no effect, and TDLDA absorption spectra are not such different from the RPA result. This can be explained by the following argument: as it can be seen in Eq. (2.14), the xc kernel only appears in a term $\chi^{\rm KS} f_{\rm xc}$ that is coupled to the Kohn-Sham polarizability $\chi^{\rm KS}$. In the optical limit $q \to 0$ the Kohn-Sham polarizability goes to 0 as $\lim_{q\to 0} \chi^{\rm KS}(q) \sim q^2 \to 0$, as it can be seen from Eq. (2.24) and knowing that $\rho^{\rm KS}_{ij}(q) \sim q \to 0$. Now a local kernel such as the ALDA behaves as a constant for $q \to 0$, $\lim_{q\to 0} f_{\rm xc}^{\rm ALDA} = {\rm const}$, such as the term $\lim_{q\to 0} \chi^{\rm KS} f_{\rm xc}^{\rm ALDA} = 0$ goes to 0 in the optical limit, and the final result cannot be too much different from the RPA $f_{\rm xc} = 0$ case. In order to have a result that starts to be different from the RPA case we should introduce a non-local contribution into the xc kernel. That was the reason why in our PhD thesis work we tried to go beyond LDA by introducing some little non-locality by a new approximation we called NLDA (see section 4.5 in Ref. [Olevano 99b]). However this small non-locality was still not enough (compare continuous line in Fig. 6.2 of Ref. [Olevano 99b]) and we realized that the true exact kernel must contain an *ultra* non-local, long-range $1/q^2$ Coulomb-like contribution. Indeed in this case the kernel diverges $f_{\rm xc} \to \infty$ in the optical limit. So that the term $\chi^{\rm KS} f_{\rm xc}$ keeps finite and the result is allowed to differ from RPA. We tried then to introduce a kernel of the form α/q^2 (pages 101 and 107 of Ref. [Olevano 99b]). The calculation (green dot-dashed line in Fig. 2.7) showed that finally the result started to be different with respect to the RPA (and ALDA) ones. For a positive ($\alpha > 0$) long-range contribution, we observed in the optical absorption a redistribution of the spectral weight toward larger energies with respect to RPA. This seemed to go in the right direction in order to improve upon the rigid red-shift due to *e-e* interaction effects and gave some hope. However the agreement with the experiment was still completely unsatisfactory. The first low-energy peak was even reduced with respect to RPA (compare Fig. 2.7 and 2.1).

The right recipe for a correct long-range xc kernel was found only successively. We indeed realized that for a kernel of the α/q^2 form would be extremely difficult to correct both the RPA drawbacks, i.e. the underestimation of the optical onset (lack of *e-e* interaction effects) and the underestimation of the low-energy spectral weight (lack of *e-h* excitonic effects). Of course, the true exact kernel should correct the Kohn-Sham independent particle polarizability $\chi^{\rm KS}$ for both effects. But it can be split into two components,

$$f_{\rm xc} = f_{\rm xc}^{e\text{-}e} + f_{\rm xc}^{e\text{-}h}, \tag{2.27}$$

the first associated to the task of reproducing *e-e* effects, the second to *e-h*. The right recipe we proposed in Ref. [Reining 02] was to start from a more advanced point, from an already *e-e* self-energy corrected independent quasiparticle $\Pi^{(0)}$, instead of an independent particle Kohn-Sham $\chi^{\rm KS}$,

$$\Pi^{(0)} = \chi^{\rm KS} + \chi^{\rm KS} f_{\rm xc}^{e\text{-}e} \Pi^{(0)}. \tag{2.28}$$

In practice, we calculated directly $\Pi^{(0)}$ using a GW electronic structure instead of a Kohn-Sham. For simple semiconductors, a shissor operator over a Kohn-Sham structure is often almost equivalent to GW. The remaining task was instead taken into account by an $f_{\rm xc}^{e\text{-}h} = f_{\rm xc}^{\rm LRC}$ long-range contribution kernel,

$$\chi = \Pi^{(0)} + \Pi^{(0)}(w + f_{\rm xc}^{e\text{-}h})\chi. \tag{2.29}$$

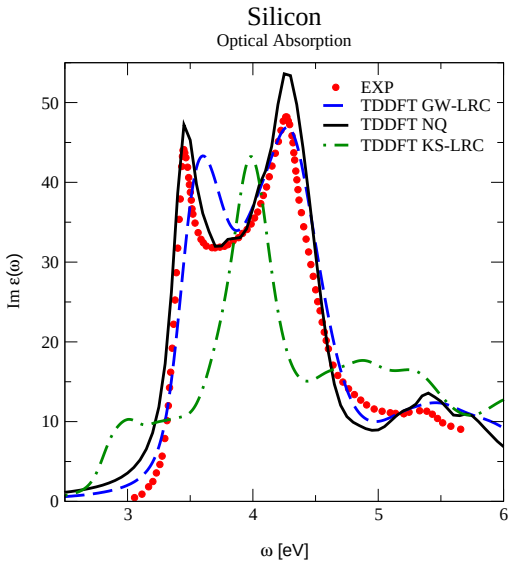

Figure 2.7: Optical absorption in silicon. Imaginary part of the macroscopic dielectric function in the LRC on top of $\chi^{\rm KS}$ (green dot-dashed line, reproducing with higher convergence solid line of Fig. 6.5 in Ref. [Olevano 99b]), LRC on top of $\Pi^{(0)}$ (blue dashed line, reproducing Fig. 1 of Ref. [Reining 02]), Nanoquanta kernel (black continuous line, reproducing Fig. 2 of Ref. [Sottile 03b]), and ellipsometry experiment (red dots from Ref. [Lautenschlager 87]).

$f_{\rm xc}^{e\text{-}h} = \alpha/q^2$ is taken of the long-range Eq. (2.25) form, but with the important novelty that the sign of the divergence is taken *negative*, $\alpha < 0$, such as to transfer oscillator weigth to lowest energies instead of highest.

The results we got on silicon [Reining 02] are presented in Fig. 2.7, blue dashed line. We remark an overall good agreement with the experiment. With respect to the GW or SO optical absorption (Fig. 2.2), the optical onset is unchanged and keeps at the good position of the photoemission band gap. However, most of the spectral weight has been transferred from high to low energy. The amplitude of the transfer is modulated by the α parameter and the direction is due to the negative sign in Eq. (2.25). The result is that now the first peak acquired strength with respect to the rest of the spectrum. This is the effect of the *e-h* interaction for materials with screening of the order of $\varepsilon_\infty \simeq 10$, that is semiconductors. In these systems *e-h* interactions are not such strong to create bound excitons within the photoemission band gap. However, they affect and strengthen the low energy part of the optical absorption spectrum. Thus, with respect to the first essay (green dot-dashed curve in Fig. 2.7), the right ingredients for a good LRC approximation are: i) start from the QP polarizability and the correct (non red-shifted) continuum optical onset; ii) apply the LRC kernel Eq. (2.25) with the minus sign, since the problem now in $\Pi^{(0)}$ is to transfer spectral weight *back* (to lowest energies).

The adjustable parameter was found to be $\alpha = -0.22$ for silicon. The problem of the approximation is that it is not any more *ab initio*, at least from a rigorous point of view. Indeed, one year later [Botti 04] we realized that

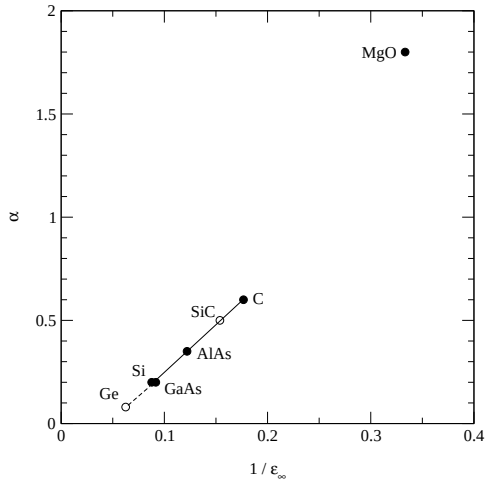

Figure 2.8: Relationship $|\alpha|$ parameter (y-axis) dielectric constant ε_∞^{-1} (x-axis) (reproducing Fig. 12 of Ref. [Botti 04]) for several materials.

the α parameter which weights the intensity of excitonic effects, is in inverse relationship with the screening, the dielectric constant ε_∞^{-1} as in the experiment or in the RPA approximation (see Fig. 2.8). This was of course expected and searched. We found that we can calculate α by the linear expression

$$\alpha = -4.615\varepsilon_\infty^{-1} + 0.213, \tag{2.30}$$

where the coefficients are a fit on the set of materials presented in Fig. 2.8. Now the approximation can be applied in a first principles way, calculating ε_∞^{-1} in the RPA approximation, then α, and finally the spectra. This approximation provides good result for semiconductors and small bandgap insulators like diamond. It breaks down for large band gap insulators (for example MgO) where the screening is so low that a simple readjustement of oscillator weight in the spectrum is not any more sufficient to reproduce the e-h interaction effect. These systems present bound excitons. A single bound exciton can be conjured using very large α, beyond Eq. (2.30). However it is difficult to reproduce the spectrum correctly at low and high energies at the same time using a single parameter α. We can in principle introduce a complication, such as a frequency dependent weight of the long-range term, as done in Ref. [Botti 05]. This frequency dependence would be also necessary to reproduce the EELS spectrum at the same time as the optical absorption. The issue of the frequency dependence is also discussed in Ref. [Del Sole 03]. I think that some more work should be done in this direction. In perspective, we could achieve a kernel not too much more complicated than Eq. (2.25), able to reproduce both bound excitons and excitonic effects over a wider range of systems, and over several energy scales, from the optical range to the EELS.

2.10 Nanoquanta kernel

The problem to have a, let's say, purer *ab initio* approach to calculate optical spectra in presence also of bound excitons, has been addressed and solved in the following years. This has led to the development and implementation of what is today called the *Nanoquanta kernel*, here written diagramatically:

$f_{xc} = \Pi^{(0)\,-1} GGWGG\Pi^{(0)\,-1} =$

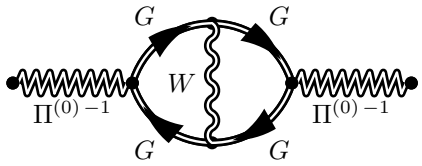

where $W = \varepsilon^{-1} w$ is the screened interaction and G is the Green's function. This kernel, written in another form in Eq. (9) of Ref. [Reining 02], was proposed as a BSE-derived TDDFT kernel able to reproduce spectra as in the Bethe-Salpeter approach with both excitonic effects and bound excitons. It was derived by L. Reining relying on the 4-point TDDFT Casida's equation, which is on the same footing as the 4-point Bethe-Salpeter equation. The derivation required the two equations to produce the same spectra. Exactly the same expression was also previously derived by R. Del Sole [Adragna 01, Adragna 03] following a different derivation, based rather on perturbation theory and using an expansion along a new direction. This expression was tested in a tight-binding framework with satisfactory results [Adragna 01]. This kernel was in the next years rederived several other times [Tokatly 01, von Barth 05, Bruneval 05, Gatti 07c] starting from different points of view with several variants. Here we propose a derivation which is a variant of the I. Tokatly and O. Pankratov [Tokatly 01] original diagramatic derivation.

Proof: We start from the Hedin's equation (3.8) for the irreducible vertex $\tilde{\Gamma}$,

$$\tilde{\Gamma} = 1 + \Xi_{\rm M} GG\tilde{\Gamma},$$

and we define

$$\tilde{\Gamma}' \stackrel{def}{=} \Xi_{\rm M} GG\tilde{\Gamma},$$

that is, $\tilde{\Gamma}' = \tilde{\Gamma} - 1$, which presents more affinity to the xc kernel. The equation for the irreducible polarizability in terms of $\tilde{\Gamma}'$ is

$$\tilde{\chi} = GG\tilde{\Gamma} = GG + GG\tilde{\Gamma}' = \Pi^{(0)} + GG\tilde{\Gamma}', \tag{2.31}$$

since $\Pi^{(0)} = GG$. Here from Eq. (2.29), $GG\tilde{\Gamma}'$ should equal $\Pi^{(0)} f_{\rm xc}^{e\text{-}h} \tilde{\chi}$. The Hedin's equation for $\tilde{\Gamma}'$ reads

$$\begin{aligned} \tilde{\Gamma}' &= \Xi_{\rm M} GG + \Xi_{\rm M} GG\tilde{\Gamma}' = \\ &= \Xi_{\rm M} GG + \Xi_{\rm M}(GG - GG\Pi^{(0)\,-1} GG)\tilde{\Gamma}' + \Xi_{\rm M} GG\Pi^{(0)\,-1} GG\tilde{\Gamma}' \end{aligned}$$

We now define the quantity $\tilde{\Lambda}'$ over which we will later do a development,

$$\tilde{\Lambda}' = \Xi_{\rm M} GG + \Xi_{\rm M}(GG - GG\Pi^{(0)\,-1} GG)\tilde{\Lambda}', \tag{2.32}$$

such as the equation for $\tilde{\Gamma}'$ takes the form

$$\tilde{\Gamma}' = \tilde{\Lambda}' + \tilde{\Lambda}'\Pi^{(0)\,-1} GG\tilde{\Gamma}'. \tag{2.33}$$

This can be checked thank to the follwoing relations:

$$(\Xi_{\rm M} GG)^{-1} = \tilde{\Gamma}'^{-1} + 1$$
$$(\Xi_{\rm M} GG)^{-1} = \tilde{\Lambda}'^{-1} + 1 - \Pi^{(0)\,-1} GG$$
$$\tilde{\Lambda}'^{-1} = \tilde{\Gamma}'^{-1} + \Pi^{(0)\,-1} GG$$

Now from Eq. (2.31) we can replace $GG\tilde{\Gamma}'$ by $\tilde{\chi} - \Pi^{(0)}$ in Eq. (2.33)

$$\tilde{\Gamma}' = \tilde{\Lambda}' + \tilde{\Lambda}'\Pi^{(0)\,-1}\tilde{\chi} - \tilde{\Lambda}'\Pi^{(0)\,-1}\Pi^{(0)} = \tilde{\Lambda}'\Pi^{(0)\,-1}\tilde{\chi}.$$

Finally

$$\tilde{\chi} = \Pi^{(0)} + GG\tilde{\Gamma}' = \Pi^{(0)} + GG\tilde{\Lambda}'\Pi^{(0)\,-1}\tilde{\chi} = \Pi^{(0)} + \Pi^{(0)}\Pi^{(0)\,-1}GG\tilde{\Lambda}'\Pi^{(0)\,-1}\tilde{\chi},$$

And comparing with Eq. (2.29), the *e-h* xc kernel turns out to be

$$f_{\rm xc}^{e\text{-}h} = \Pi^{(0)\,-1}GG\tilde{\Lambda}'\Pi^{(0)\,-1}.$$

Using for $\tilde{\Lambda}'$ its first order in the development Eq. (2.32), or better its first iteration,

$$\tilde{\Lambda}' = \Xi_{\rm M} GG,$$

we arrive at the end to

$$f_{\rm xc}^{e\text{-}h\ (1)} = \Pi^{(0)\,-1}GG\Xi_{\rm M}GG\Pi^{(0)\,-1} \simeq \Pi^{(0)\,-1}GGWGG\Pi^{(0)\,-1},$$

which is the Nanoquanta kernel ■

The Nanoquanta kernel has been implemented by F. Sottile during his PhD thesis [Sottile 03a], overcoming many difficulties. In particular, the problem to invert the polarizability $\Pi^{(0)\,-1}$ which does not exist at frequencies where the polarizability presents a 0 eigenvalue. This led to divergencies in the xc kernel, seen as spikes in the final spectra. The problem has been solved by introducing the less pathological quantity

$$T = \Pi^{(0)} f_{\rm xc}^{e\text{-}h}\Pi^{(0)} = GGWGG, \tag{2.34}$$

and rather solving a TDDFT equation of the form

$$\chi = \Pi^{(0)}(\Pi^{(0)} - \Pi^{(0)}w\Pi^{(0)} - T)^{-1}\Pi^{(0)},$$

instead of Eq. (2.29). Indeed, the xc kernel is not an observable, and it appears in expressions leading to observables quantities always in the form Eq. (2.34). So that in principle it can be a non-analytic function.

The Nanoquanta kernel result [Sottile 03b] obtained for silicon is shown in Fig. 2.7 (black line). We remark again the good agreement with the experiment (and of course with the BSE result, by construction). In Fig. 2.9 we show the result [Sottile 07] for solid argon, a system presenting a series of bound excitons. The Nanoquanta kernel, like the Bethe-Salpeter approach, is able to reproduce the complete series of 3 peaks associated to bound excitons, while the RPA and GW-RPA results completely fail. Ref. [Sottile 07] also discuss aspects related to an improved algorithm to calculate the kernel. Notice that this Nanoquanta approach have also studied the other term of the xc kernel, namely the *e-e* interaction kernel $f_{\rm xc}^{e\text{-}e}$, and shown that a kernel doing the job to reproduce self-energy effects effectively exists. The drawback is that to calculate this kernel the GW electronic structure must be calculated in advance. Which is what one would like to avoid in order to keep within a, let's say, as much as pure density-functional theory as possible.

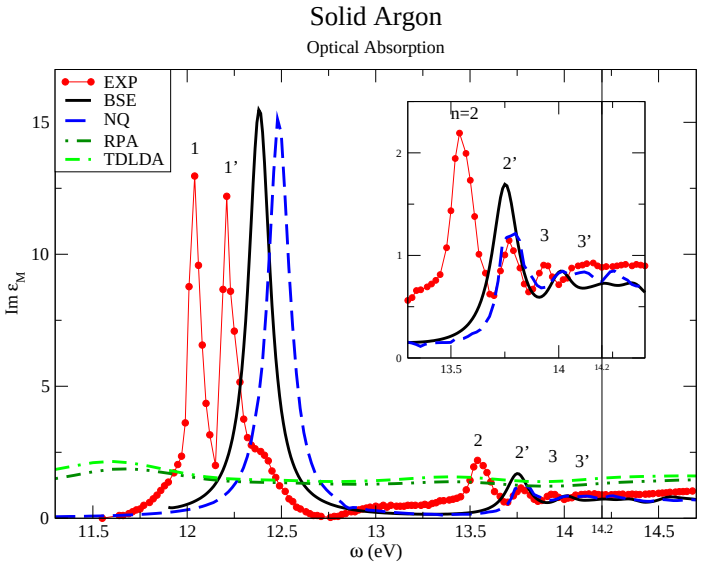

Figure 2.9: Optical absorption in solid argon (from Ref. [Sottile 07]). Red line and dots: experiment; blue dashed line: Nanoquanta (NQ) kernel; black continuous line: Bethe-Salpeter (BSE) result; green double-dashed-dotted line: TDLDA; green double-dotted-dashed line RPA. There are two exciton series, the spin triplet n and the singlet n'. Non spin-polarized calculations are supposed to reproduce only the spin singlet n' series. The bandgap is 14.2 eV in Argon.

2.11 Perspectives beyond the Nanoquanta kernel

Although with the Nanoquanta kernel we succeeded in having a truly *ab initio* kernel able to reproduce all neutral excitations and spectra, yet fundamental criticisms persist. The first one is that this approach still is in the path of OEP schemes for DFT or TDDFT. Indeed, the expression for the kernel is still orbital dependent with complicated expressions. Regarding this last point, we however have shown [Sottile 07] that the scaling on evaluating the exchange-correlation expression is much better than in OEP approaches.

Another fundamental criticism [Gross 03] is that the Nanoquanta scheme looks a hybrid MBQFT/DFT approach. The kernel is separated into two terms: one reproducing self-energy effects, whose effect reproduce an independent quasiparticle polarizability, a kind of non-interacting polarizability built however over an interacting (quasiparticle) electronic structure. The second term introduces vertex corrections to the polarizability so to keep into account e-h interaction effects, thus allowing to reproduce excitons and excitonic effects in optical spectra. This separation looks [Gross 03] quite artificial and is not truly in the spirit of a density-functional like theory that does not deal with self-energies and vertex functions. Further on, although we provided an explicit expression for the excitonic term of the kernel, the first term is still implicit. This means that to do a Nanoquanta kernel calculation, one needs to

first calculate GW corrections to the Kohn-Sham energies. Apart to be in some cases the most cumbersome step, this means that the theory is not completely self-standing as density-functional approach.

Although it has been important to show that TDDFT is able to provide from *ab initio* optical spectra in good agreement with the experiment, all the above drawbacks would require further work. I do not personally consider the problem as definitely solved. And I think that this could still continue to be an exciting field of research for us and of course for the new generations of condensed matter theoreticians.

Chapter 3

MBQFT, GW approximation and beyond

In this chapter we introduce the fundamentals of MBQFT and the GW approximation. The main achievements of the theory, in particular the *ab initio* prediction of band gaps in insulator and semiconductors as measured in ARPES, are discussed. We analyze two examples among recent work by us: the first is a fully dynamical GW calculation on graphene, for some aspects quite an exotic system. This is a work whose main author is Paolo Emilio Trevisanutto, at that time Post-Doc in my laboratory. The second is a self-consistent GW calculation on VO_2, work carried out in particular by Matteo Gatti during his PhD thesis [Gatti 07a] under the supervision of Lucia Reining and myself. These works point to the next challenges in front of the GW approximation: the access to spectral functions and the description of strongly-correlated systems. On ordinary insulators, semiconductors and metals, the GW approximation has so far provided good results. However nobody knows how GW will perform on systems where the band paradigm breaks down as in the strongly correlated phenomenology. These systems hence represent the next frontier for GW. In any case, since GW is an approximation, we must expect a limit beyond which its validity is lost. And this could be situated at the level of strong correlations. If we want to depass this frontier keeping within an *ab initio* approach, we should be able to devise new approximations beyond GW, toward vertex corrections. Along this path, great help will come from the physics learnt from strongly correlated models, e.g. the Hubbard model. Finally, starting from an idea raised during Matteo Gatti's thesis, we present developments even beyond MBQFT, toward a simpler framework although still in principle exact for excitations. We have in mind an intermediate framework between DFT and MBQFT, rather than a hybrid of the two, like in OEP approaches.

3.1 Second quantization and Fock space

The starting point of MBQFT and any quantum field theory is the introduction of second quantization. In the second quantization formalism the ordinary

wavefunction becomes an operator,

$$\psi(r) \longmapsto \hat{\psi}(r),$$

acting on the *Fock space* which is a Hilbert space of the occupation numbers. In this space a possible state is the vacuum, $|0\rangle$, that is the ground-state of QED or other subnuclear field theories. Another example is the state where it is present one electron with energy E and momentum p, $|1_{E,p}\rangle$. In condensed matter we introduce the ground-state of an N-electron system $|\Psi_0^N\rangle$ as well as its excited states $|\Psi_s^N\rangle$. Charged excited states are obtained from the N-electron ground-state by e.g. adding $|\Psi_0^{N+1}\rangle$ or removing $|\Psi_0^{N-1}\rangle$ an electron. The field operator $\hat{\psi}(r)$ is defined as the operator that removes an electron at r from a Fock state, while its conjugate $\hat{\psi}^\dagger(r)$ creates an electron at r. This is a tool formerly introduced by Paul Dirac to reformulate the problem of the harmonic oscillator. Field operators obey canonical commutation/anticommutation relations, according to their bosonic/fermionic statistics and in agreement with the spin-statistics theorem. So, for electrons

$$\begin{aligned}
&\{\hat{\psi}(r), \hat{\psi}(r')\} = 0 \\
&\{\hat{\psi}^\dagger(r), \hat{\psi}^\dagger(r')\} = 0 \\
&\{\hat{\psi}(r), \hat{\psi}^\dagger(r')\} = \delta(r, r').
\end{aligned}$$

These relations are enough to automatically impose fermionic antisymmetrization everywhere in the theory (point 2. in Sec. 1.2). A first interesting second quantized operator that can be introduced is the electronic density operator,

$$\hat{\rho}(r) = \hat{\psi}^\dagger(r)\hat{\psi}(r),$$

whose mean value on a generic state provides the electronic density observable,

$$\rho(r) = \langle\Psi|\hat{\rho}(r)|\Psi\rangle.$$

The total number of particles operator is instead

$$\hat{N} = \int dr\, \hat{\rho}(r) = \int dr\, \hat{\psi}^\dagger(r)\hat{\psi}(r).$$

A generic $o(r, \partial_r)$ first quantization single-particle operator, which would be $o = \sum_{n=1}^{N} o(r_n, \partial_{r_n})$ for an N particle system, always possesses an associated second quantization expression,

$$\hat{o} = \int dr\, \hat{\psi}^\dagger(r) o(r, \partial_r) \hat{\psi}(r).$$

From the last expression, we see that in a field theory there is not any more need to deal with indeces running on the entire set of particles (point 1. in Sec. 1.2). Indeed, the many-body hamiltonian Eq. (1.1) is in second quantization

$$\hat{H} = \hat{H}^{(0)} + \hat{W} = \hat{T} + \hat{V} + \hat{W} \tag{3.1}$$

$$\hat{T} = \int dr\, \hat{\psi}^\dagger(r) \left(-\frac{1}{2}\partial_r^2\right) \hat{\psi}(r) \tag{3.2}$$

$$\hat{V} = \int dr\, \hat{\psi}^\dagger(r) v(r) \hat{\psi}(r) \tag{3.3}$$

$$\hat{W} = \frac{1}{2} \int dr dr'\, \hat{\psi}^\dagger(r)\hat{\psi}^\dagger(r') w(r, r') \hat{\psi}(r')\hat{\psi}(r) \tag{3.4}$$

where, with respect to Eq. (1.1) the index n running on the total number of particles N, has disappeared.

3.2 Green's function

We can now define the Green's function. The time-ordered 0-temperature single-particle Green's function is the expectation value on the ground-state of the operator[1] $T\{\hat{\psi}(r_1,t_1)\hat{\psi}^\dagger(r_2,t_2)\}$,

$$G(r_1,t_1,r_2,t_2) = -i\langle\Psi_0^N|T\{\hat{\psi}(r_1,t_1)\hat{\psi}^\dagger(r_2,t_2)\}|\Psi_0^N\rangle, \tag{3.5}$$

where T is the time-ordering product, defined (for fermions) as

$$T\{\hat{o}(t_1)\hat{o}^\dagger(t_2)\} = \begin{cases} \hat{o}(t_1)\hat{o}^\dagger(t_2) & t_1 > t_2 \\ \pm\hat{o}^\dagger(t_2)\hat{o}(t_1) & t_2 > t_1 \end{cases}.$$

The Green's function has the following interpretation: it represents the probability amplitude to detect an electron at point r_1 and time t_1 when an electron has been added to the system at a point r_2 and in a previous time t_2. It hence represents the probability amplitude for the propagation of the electron from r_2, t_2 to r_1, t_1. This is the reason why the Green's function is also called *propagator*. When $t_2 > t_1$, the Green's function describes the propagation of a many-body state in which an electron has been removed in r_1, t_1, that is the propagation of a hole from r_1, t_1 to r_2, t_2.

To clarify its meaning, it can be usefull to study the Green's function of the simple non-interacting system $\hat{H}^{(0)}$, characterized by a single-particle Hamiltonian $h^{(0)}$ and eigenvalues/vectors $\epsilon_i^{(0)}$, $\phi_i^{(0)}(r)$. From the definition Eq. (3.5), we can see that the *independent-particle* Green's function $G^{(0)}$ obeys an equation,

$$\left[i\partial_{t_1} - h^{(0)}(r_1)\right] G^{(0)}(x_1,x_2) = \left[i\partial_{t_1} + \frac{1}{2}\partial_{r_1}^2 - v(r_1)\right] G^{(0)}(x_1,x_2) = \delta(x_1,x_2),$$

which is the ordinary mathematical definition for the Green's function of the differential operator $i\partial_t - h^{(0)}(r)$. In $r\omega$-space, that is Fourier transforming with respect to $(t_2 - t_1) \to \omega$, the Green's function is equal to

$$G^{(0)}(r_1,r_2;\omega) = \sum_i \frac{\phi_i^{(0)}(r_1)\phi_i^{(0)*}(r_2)}{\omega - \epsilon_i^{(0)} + i\eta\,\mathrm{sgn}\left(\epsilon_i^{(0)} - \mu\right)}. \tag{3.6}$$

where μ is the chemical potential. We can see that the Green's function contains several informations and in particular:

1. The expectation value of any single-particle operator on the ground-state.
2. The ground-state total energy.
3. The excitation spectrum.

[1] From now on we will use the Heisenberg representation in which the time-dependence is trasferred from the (Fock) states to the second-quantized operators.

Indeed it can be shown that a generical observable associated to a single-particle first quantization operator $o(r, \partial_r)$ (point 1.) can be calculated from the Green's function via

$$o(t) = -i \int dr \lim_{r' \to r} \lim_{t' \to t^+} o(r, \partial_r) G(r, t, r', t').$$

Although the total energy (the Hamiltonian) contains the two-particle operator W, nevertheless the ground-state total energy can be calculated from the Green's function (point 2.) by the Galtitskii-Migdal formula [Fetter 71] ($x = (r, t)$):

$$E = -\frac{1}{2} \int dr \lim_{x' \to x^+} \left[i\partial_t - \frac{1}{2}\partial_r^2 + v(r) \right] G(x, x').$$

Finally the poles of the Green's function are the excitation energies ϵ_i of the system (point 3.). This can be seen in the non-interacting system from Eq. (3.6), and in the more general case by expressing the Green's function in the Lehmann representation [Fetter 71]

$$G(r_1, r_2, \omega) = \sum_s \frac{\psi_s(r_1)\psi_s^*(r_2)}{\omega - \epsilon_s + i\eta \,\mathrm{sgn}(\epsilon_s - \mu)}$$

where the ϵ_s are the *charged* excitations, either particle or hole, of the N-particle system, and the $\psi_s(r)$ are the so-called Lehmann amplitudes.

Another important observable can be directly extracted from the Green's function. This is the *spectral weight function* $A(\omega)$ (or spectral function) which can be defined as

$$A(r_1, r_2, \omega) = \sum_s \psi_s(r_1)\psi_s^*(r_2)\delta(\omega - \epsilon_s).$$

The spectral function has the meaning of a weighted density-of-states for the full interacting many-body system, and can be calculated by taking the imaginary part of the Green's function

$$A(r_1, r_2, \omega) = -\pi^{-1} \Im G(r_1, r_2, \omega) \,\mathrm{sgn}(\omega - \mu)$$

The diagonal of the reciprocal space spectral function $A_{GG}(k, \omega)$ is an observable directly measured in angle-resolved photoemission spectroscopy (ARPES). Most of the peaks present in the spectral function $A(\omega)$ are associated to *quasiparticle* excitations. These are excitations with a single-particle character but with a renormalized energy ϵ_i^{QP} (different from the independent particle energy $\epsilon_i^{(0)}$) and possessing an imaginary part to be associated to the inverse lifetime of the excitation. Some other peaks belong to the non-coherent part of the spectrum and are instead satellites associated to *collective* and delocalized excitations, such as plasmons (seen in PES spectra at multiples of the plasma frequency distance from the quasiparticle peaks). Or also to peaks associated to *localized* excitations, such as the so-called Hubbard bands.

3.3 Equations of motion for G and MBPT

Once we have the Green's function, all the observables can be calculated. The problem is now how to calculate G for the interacting system. This can be done

solving the equation of motion for G,

$$\left[i\partial_{t_1} + \frac{1}{2}\partial^2_{r_1} - v(r_1)\right] G(x_1, x_2) + i \int dx_3\, w(x_1, x_3) G(x_1, x_3^+, x_2, x_3^{++}) = \delta(x_1, x_2), \tag{3.7}$$

that requires knowledge of the 2-particle Green's function $G(x_1, x_2, x_3, x_4)$. This is defined analogously to the 1-particle Green's function with 4 field operators and is a function of 4 space-time points. In turn the equation of motion for the 2-particle G requires knowledge of the 3-particle G and so on. Along this way the problem has no solution[2].

One possible way is to use *perturbation theory* by considering as 0-order the independent-particle Hamiltonian $\hat{H}^{(0)}$ which represents a problem that we can solve. We know how to calculate its Green's function $G^{(0)}$ Eq. (3.6). We then consider as perturbation the many-body term $\hat{W}$ and the Coulomb e-e repulsion $w(r, r')$. Using Wick's theorem, we can expand the T-product in the definition of the Green's function into normal products and contractions on the ground-state, and expand G till a given order of W in terms of $G^{(0)}$. G can be written in terms of Feynman diagrams and can be calculated up to a desired order. This is the way followed to solve the problem in QED and was the first trial to solve MBQFT. Unfortunately, while in QED the coupling constant around which we expand the theory is small, in MBQFT this is not the case. The situation is like in QCD at the low-energies scale, where the strong constant is not small. In many-body perturbation theory (MBPT) the first order corresponds to Hartree-Fock theory which is not a good approximation, as we already know, especially in solids or infinite systems. Second and further orders are not small with respect to the first, and stopping at a given order cannot represent systematically a good choice to minimize the error. The error is not under control. In historical order, the next developments of MBPT went toward partial resummation to all orders along some chosen directions of Feynman diagrams. For example, summing all the ring diagrams (RPA approximation). Or summing to all orders ladder-like Feynman diagrams (ladder approximation). All these approches failed to provide a systematically correct methodology to the many-body problem.

3.4 The self-energy and Hedin's equations

There is another way to solve the problem called *functional* or also *iterative* approach. The functional appoach consists in disentangling the series of dependencies of the G in Eq. (3.7) over the 2-particle or further Gs by introducing a new quantity called *self-energy*. The irreducible self-energy $\tilde{\Sigma}$ is defined implicitly by a newly introduced equation of motion for the 1-particle G,

$$\left[i\partial_{t_1} + \frac{1}{2}\partial^2_{r_1} - v(r_1)\right] G(x_1, x_2) - \int dx_3\, \tilde{\Sigma}(x_1, x_3) G(x_3, x_2) = \delta(x_1, x_2).$$

In this equation the self-energy sums up to the external potential $v(r)$ and thus acquires the meaning of an *effective* potential accounting for the many-body interaction ($\tilde{\Sigma} = 0$ for the non-interacting system). This interpretation is

[2] One can solve the problem by doing approximations for example on the 2-particle G, writing it as a functional expression involving the 1-particle G and w. This is equivalent to do a perturbation theory of G over $G^{(0)}$ and w, which is discussed in the next.

reinforced knowing that we can write a Schrödinger-like single-particle equation for the interacting *quasielectron*,

$$\left[i\partial_{t_1} + \frac{1}{2}\partial^2_{r_1} - v(r_1) - v_{\rm H}(r_1)\right]\psi_i^{\rm QP}(x_1) - \int dx_3\, \tilde{\Sigma}_{\rm M}(x_1,x_3)\psi_i^{\rm QP}(x_3) = \epsilon_i^{\rm QP}\psi_i^{\rm QP}(x_1),$$

where the self-energy has been decomposed into $\tilde{\Sigma}(x_1,x_2) = \delta(x_1,x_2)v_{\rm H}(x_1) + \tilde{\Sigma}_{\rm M}(x_1,x_2)$, the Hartree potential $v_{\rm H}(x_1) = \int dx_3\, \rho(x_3)w(x_3,x_1)$, representing the classical repulsion felt by the electron and due to all the other electrons, and the *mass-operator* $\tilde{\Sigma}_{\rm M}$, rather associated to quantistic effects. So far everything is exact. The exact self-energy is a function of two space-time variables x_1, x_2. We can approximate the self-energy by a local potential, for example neglecting the rest beyond the local Hartree potential $v_{\rm H}(x)$. This is equivalent to the Hartree theory and it is a kind of classical *mean-field theory* where the self-energy acquires the function of an effective potential. In the Hartree-Fock approximation we approximate $\tilde{\Sigma}_{\rm M}$ by the exchange operator $\tilde{\Sigma}_{\rm x}$, i.e. $\tilde{\Sigma}^{\rm HF}_{\rm M}(x_1,x_2) = \tilde{\Sigma}_{\rm x}(x_1,x_2) = \int dx_3\, G(x_1,x_3)w(x_3,x_2)$. In the exact theory, $\tilde{\Sigma}_{\rm M} = \tilde{\Sigma}_{\rm x} + \tilde{\Sigma}_{\rm c}$ contains not only the exchange, but also *correlation* $\tilde{\Sigma}_{\rm c}$, whose rigorous definition is indeed "the contribution beyond the exchange and the Hartree-Fock approximation".

The quasiparticle energies $\epsilon_i^{\rm QP}$, eigenvalues of Eq. (3.4), represent excitations of the full interacting system of the single-particle type, that is they can be traced back, associated to single-particle excitations $\epsilon_i^{(0)}$ of the non-interacting system. Since the self-energy is not in general a Hermitian operator, the right eigenvalues $\epsilon_i^{\rm QP}$ of Eq. (3.4), at difference with the $\epsilon_i^{(0)}$, can possess also an imaginary part: the inverse of the imaginary part is associated to the lifetime $\tau_i^{\rm QP} = 1/2\Im\epsilon_i^{\rm QP}$ of the excitation, while the real part is its energy. It can be shown that the spectral function $A(\omega)$ presents peaks at $\omega = \Re\epsilon_i^{\rm QP}$ of width $\Im\epsilon_i^{\rm QP}$. In a solid the set of $\Re\epsilon^{\rm QP}_{i=nk}$ can be plot as a function of the wave-vector k, and this is the band-plot of the real interacting system as measured in ARPES.

The problem has now been transferred from the Green's function to the new unknown self-energy. We need to find an equation of motion for it. The idea is that we can repeat the procedure, introduce new equations and new quantities in the hope that, unlike for many-particle Green's function, we succeed in closing the set of equations. This procedure leads to the so-called Hedin's equations [Hedin 65], a set of 5 closed integro-differential equations over 5 unknowns:

$$\begin{aligned}
G(x_1,x_2) &= G^{(0)}(x_1,x_2) + \int dx_3\, dx_4\, G^{(0)}(x_1,x_3)\tilde{\Sigma}(x_3,x_4)G(x_4,x_2)\\
W(x_1,x_2) &= w(x_1,x_2) + \int dx_3\, dx_4\, w(x_1,x_3)\tilde{\Pi}(x_3,x_4)W(x_4,x_2)\\
\tilde{\Sigma}_{\rm M}(x_1,x_2) &= i\int dx_3\, dx_4\, W(x_1^+,x_3)G(x_1,x_4)\tilde{\Gamma}(x_4,x_2;x_3)\\
\tilde{\Pi}(x_1,x_2) &= -i\int dx_3\, dx_4\, G(x_1,x_3)\tilde{\Gamma}(x_3,x_4;x_2)G(x_4,x_1^+)\\
\tilde{\Gamma}(x_1,x_2;x_3) &= \delta(x_1,x_3)\delta(x_1,x_2) +\\
&\quad + \int dx_4\, dx_5\, dx_6\, dx_7\, \frac{\delta\tilde{\Sigma}_{\rm M}(x_1,x_2)}{\delta G(x_4,x_5)}G(x_4,x_6)G(x_7,x_5)\tilde{\Gamma}(x_6,x_7;x_3)
\end{aligned}$$

where we have introduced other 4 quantities: the irreducible polarizability $\tilde{\Pi}$, directly related to the macroscopic polarizability of the system; the screened interaction W, which is the Coulomb interaction screened by the dynamical dielectric function of the medium, $W(\omega) = \varepsilon^{-1}(\omega)w$, directly related to the effective interaction of two electrons in presence of all the others; and the irreducible vertex function $\tilde{\Gamma}$, of more difficult physical interpretation. $G^{(0)}$ is of course the well known Green's function of the non-interacting system, and the first equation is called the Dyson equation, directly derived from the definition of the self-energy Eq. (3.4). The set of Hedin's equations can be solved *iteratively* and *self-consistently*, by starting from an initial guess for a quantity, say $\tilde{\Sigma}$, and solving one after the other all the equations until we get an improved, first-iteration expression for all the quantities. At this point we cycle again the 5 equation until the quantities do not change any more and convergence has been achieved on them. At this point we have the *exact* Green's function of the system and we can calculate all the observables.

Unfortunately this approach can be applied only to simple models, such as the jellium [Holm 98]. For real system the resolution of Hedin's equations turned out unfeasable. In particular, the most serious problem is posed by the last equation for the vertex $\tilde{\Gamma}$ Eq. (3.8), since the kernel of the equation is represented by the functional derivative of the self-energy with respect to the Green's function $\Xi_{\mathrm{M}} = \delta\tilde{\Sigma}_{\mathrm{M}}/\delta G$ which cannot be done analitically and it is difficult to carry out numerically. However we can now resort to approximations in the hope that, within this functional scheme, they would work better than in perturbation theory. Indeed, judicious approximations on the functional expression of the self-energy have been found so to select the most important contributions and neglect small corrections to the main physics.

3.5 The GW approximation

A succesful approximation on the self-energy is represented by the GW approximation [Hedin 65] In this approximation we simplify the complicated vertex Eq. (3.8) by retaining only its first term, the bare vertex,

$$\tilde{\Gamma}^{\mathrm{GW}}(x_1, x_2; x_3) = \delta(x_1, x_2)\delta(x_1, x_3),$$

and neglect the second term and the complicated functional derivative. The equation for the self-energy in the GW approximation then reads

$$\tilde{\Sigma}^{\mathrm{GW}}_{\mathrm{M}}(x_1, x_2) = iG(x_1, x_2)W(x_1^+, x_2),$$

expression which is eponym to the approximation. A heuristic justification of the approximation is that we are neglecting the variations $\delta\tilde{\Sigma}_{\mathrm{M}}$ of the self-energy with respect to variations induced by many-body effects on the density $\delta\rho(x) \sim \delta G(x, x)$. Another justification have been given by Mahan and Sernelius [Mahan 89], but the most important justification is provided by the *a posteriori* verification of the validity of the GW approximation on real systems by comparing with the experiment. Hedin's equations are now much easier to solve and we can at least perform a first iteration cycle along them. A self-consistent resolution of Hedin's equation even in the GW approximation can also represent a problem. So that a possibility to be seriously taken into account for real systems is to stop after the first iteration. This is called the G^0W^0 approximation.

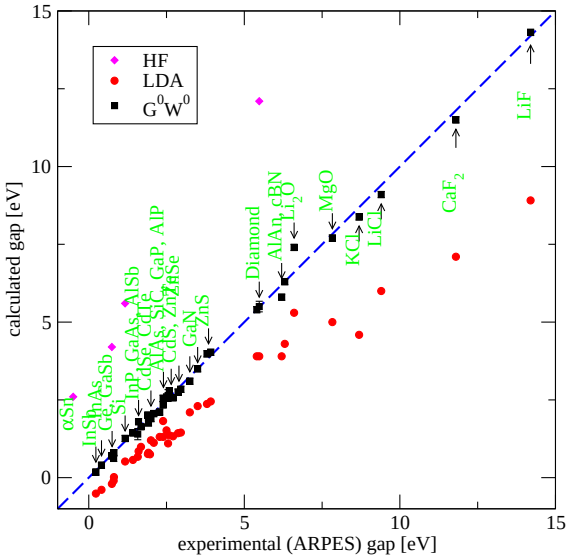

Figure 3.1: Hartree-Fock (HF, magenta diamonds), DFT-LDA (red circles) and GW (black square) calculated (y-axis) versus photoemission experimental (x-axis) band-gaps.

Its validity depends in this case also on a right choice of the starting 0-iteration point. This is normally taken to be the Kohn-Sham electronic structure, which is the simplest and best guess for an electronic structure to start with. The 0-iteration guess for the self-energy is hence taken to be the exchange-correlation functional of DFT, $\tilde{\Sigma}^0_{\rm M}(r_1, r_2, \omega) = v_{\rm xc}(r_1)\delta(r_1, r_2)$.

The most striking evidence of the validity of the G^0W^0 approximation and all this approach is provided by Fig. 3.1. Here we report the GW calculated values (ordinate) of the band-gaps in several systems, from metals to semiconductors and insulators, compared to the values measured in photoemission (abscissa). We remark the well known underestimation of DFT (in LDA or GGA approximation). It is evident that the GW approximation results lye much more along the diagonal, thus systematically improving upon DFT. Hartee-Fock band-gaps sistematically overestimate the experimental values.

3.6 Many-body GW effects on graphene

We have seen that the GW approximation typically provides band-gaps in very good agreement with ARPES experiments in systems like simple semiconductors and insulators. Let's see how GW works on an atypical system such as graphene. Graphene is a single layer/sheet of graphite, so that it has a flat 2D atomic honeycomb hexagonal lattice atomic structure. In the tight-binding formalism, the graphene 2D honeycomb lattice structure gives rise to a semimetal, that is a semiconductor with zero band gap occurring at the K point in the Brillouin zone and a cone-like linear band-dispersion at low energy. This part is usually described by a massless Weyl fermions dis-

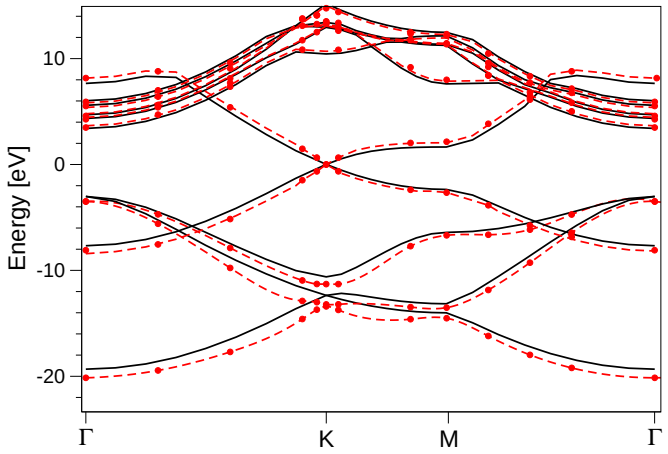

Figure 3.2: Graphene band plot (from Ref. [Trevisanutto 08]). DFT-LDA KS (black continuous lines) and GW (red dashed lines and dots) bands.

persion, $H = -\mathbf{k} \cdot \sigma$. *Ab initio* DFT calculations [Calandra 07] confirm the linear dispersion picture and give an estimate of the Fermi velocity v_F lower by 15∼20% than the experimental value. Recently, two angle-resolved photoemission spectroscopy (ARPES) experiments on graphene epitaxially grown on SiC [Bostwick 07, Zhou 07, Rotenberg 08, Zhou 08] raised the general interest. The first one [Bostwick 07, Rotenberg 08] observed at low energy a nearly linear band dispersion with slight deviations in the form of small kinks interpreted as due to many-body electron-electron (*e-e*) and electron-phonon (*e-ph*) self-energy effects. The second one [Zhou 07, Zhou 08] provided a different picture, with the opening of a band gap occurring at the Dirac K point and attributed either to substrate (SiC) or to many-body self-energy effects. A DFT calculation [Kim 08] seemed to confirm a substrate induced symmetry breaking, but recent STM measures [Brihuega 08] provided some evidence to exclude it. This situation calls for clarification about the role of *e-e* self-energy effects on the quasiparticle (QP) band plot, the Fermi velocity and the band gap opening. Previous *ab initio* works have dealt with *e-ph* effects [Calandra 07, Park 07]. There are also several non *ab initio* works (see Ref. [Neto 09] and references therein) which studied *e-e* self-energy effects in a 2D massless Dirac model.

P. E. Trevisanutto, at that time post-doc in my laboratory, and me decided to perform a GW many-body calculation in order to clarify all the previous questions. Our results [Trevisanutto 08] are shown in Fig. 3.2. We compare the Kohn-Sham DFT-LDA (black thick lines) and the quasiparticle GW (red circles and dashed lines) electronic structures. Exchange end correlations effects slightly affect the band shapes. Relevant effects are a lowering of the σ bands and an increase (up to +20%) of the gaps at M ($4 \rightarrow 4.8$ eV) and at Γ ($6.4 \rightarrow 7$ eV). This is a normal behavior of GW, as we have seen. The Kohn-Sham bands however present a qualitative good shape. We now focus on the Fermi energy Dirac point (K) region (Fig. 3.3). The DFT KS π and π^* (thick lines) band dispersion is linear in the first ~ 0.5 Å^{-1} from the Dirac K point. The DFT KS Fermi velocity is $0.95 \cdot 10^6$ ms^{-1}, in agreement with previous calculations

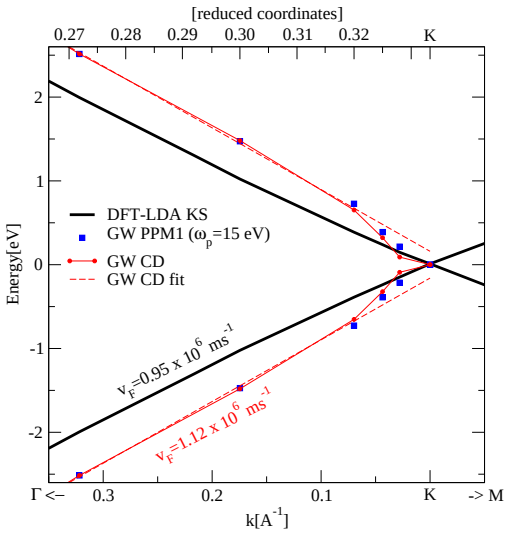

Figure 3.3: Graphene band plot zoom on the Fermi energy, K Dirac point region (from Ref. [Trevisanutto 08]): DFT-LDA KS (black lines) and GW (red lines and dots). Red dashed lines represent a fit of the Fermi velocity for the GW bands in the linear region.

[Calandra 07]. This underestimates by a 15% the experimental value. The dots and thin lines represent the GW band plot calculated by a contour deformation (CD) method. The first evident self-energy effect is the loss of linearity along the region 0.05 Å^{-1} close to the Dirac K point. However outside that region the linearity is soon recovered but with a slope larger than the DFT KS. A fit of the GW band with a straight line (dashed line) gives a Fermi velocity of $1.12 \cdot 10^6$ ms^{-1} (1.14 with $a_{\text{th}} = 2.45$ Å). Thus the GW self-energy *renormalizes* by a +17% the DFT Fermi velocity and achieves a good agreement with the experimental magnetotransport measure of $1.1 \cdot 10^6$ ms^{-1}. The residual overestimation of 2∼4% should be compensated by negative *e-ph* renormalization effects, which has been evaluated to −4% in Ref. [Park 07].

We now focus on the non-linear region. In all the k-points far from the Dirac point, the GW correction acts in the usual direction to open the gap between DFT KS bands. On the other hand at $k = (0.328, 0.328, 0)$ (reduced coordinates), that is at ~ 0.025 Å^{-1} from K, we have found an unusual *negative GW correction* of −0.12 eV which generates a *kink* at ∼ 0.1 eV from the Dirac point. This result reproduces the experimental ARPES scenario of Ref. [Bostwick 07] where a kink interpreted as due to *e-e* many-body effects is found more or less in this position. The other experimental kink has been already reproduced by an *e-ph* calculation [Calandra 07].

The last important result of our GW calculation is that many-body effects, within the numerical error bar, do not open the band gap at the Dirac point. The GW self-energy does not change the DFT-LDA 0 band gap and band 4 and 5 keep degenerate at K. In conclusion, *e-e* interaction many-body effects, at least as accounted by the GW approximation, are unable to open a band-gap and graphene keeps to be a semimetal.

3.7 GW on a strongly correlated system: VO_2

From the previous example and Fig. 3.1 we have seen how large is the domain of applicability of the GW approximation. The question now arises whether the GW is able to capture the physics of strongly-correlated systems such as in transition-metal oxydes. A prototype for such a material is vanadium dioxide (VO_2). At high temperature this oxide is in a rutile metallic phase. At 340 K it undergoes a transition to a monoclinic insulator. In the transition, the V atoms dimerize and the V pairs tilt around the rutile c-axis. It has long been debated, dating back to Nevill Mott himself [Zylbersztejn 75], whether the electronic correlation is strong enough to localize the electrons and form a Mott-Hubbard insulator [Zylbersztejn 75], or whether the structural distortions alone are enough to induce the insulating phase (Peierls model) [Wentzcovitch 94]. On this system, DFT yields ground state properties correctly. The lattice parameters and the atomic positions are in agreement with the experiment within the usual 1% error, as we also have found in our calculation [Gatti 07b]. However the Kohn-Sham DFT structure incorrectly predicts both phases to be metallic [Wentzcovitch 94, Eyert 02]. But we remind that this cannot be considered a failure of DFT, since it is not an in principle exact theory to predict excited state properties and so it is not supposed to predict the metallic/insulator character of a system. Even beyond KS-LDA, most state-of-the-art theoretical approaches were unable to describe this complex transition. Single-site DMFT gives the insulating phase as metallic [Liebsch 05, Laad 06]. In LDA+U instead even the metallic rutile structure becomes an insulator [Liebsch 05, Korotin 02]. On the other hand, a cluster-DMFT [Biermann 05] has been able to reproduce the correct character of both phases and was also able to address a peak which is clearly visible at 1.3 eV in the photoemission spectrum (PES) of the metallic phase. Into this approach, correlations are introduced by an adjustable, non *ab initio* Hubbard-model on-site parameter U. For all these reasons, no final conclusion could be drawn from first principles concerning the metal-insulator transition in VO_2 and the corresponding nature of its electronic structure.

We hence decided to carry out a fully *ab-initio* GW calculation. Our results [Gatti 07b] show that correlation effects in the electronic structure of both the metallic and the insulating phases are correctly reproduced *provided that* quasiparticle energies and wavefunctions are calculated self-consistently. So from the point of view of GW, apart from the request of self-consistence in the calculation, the situation in VO_2 is not very much more complicated as for example in germanium. Ge is a metal in the DFT KS electronic structure, but is correctly predicted to be a semiconductor with a 0.6 eV band-gap in G^0W^0.

In Fig. 3.4 we show the density of states for monoclinic VO_2 as measured by a photoemission experiment (red line). The DFT-LDA Kohn-Sham density of states (blue dashed line) is non-zero at the Fermi level, thus wrongly predicting the monoclinic phase to be metallic. A G^0W^0 on top of the DFT-LDA Kohn-Sham electronic structure does not succeed to open the band-gap and predict the phase to be metallic as well. It is only a G^0W^0 on top of a self-consistent COHSEX (a static approximation to GW with an instataneous screened interaction W) that the phase is correctly described as an insulator with a band-gap of 0.65 eV, in good agreement with the experimental 0.6 eV. In order to identify the origin of this result, we have verified that a COHSEX calculation where the wavefunctions are constrained to the LDA ones and only the energies are up-

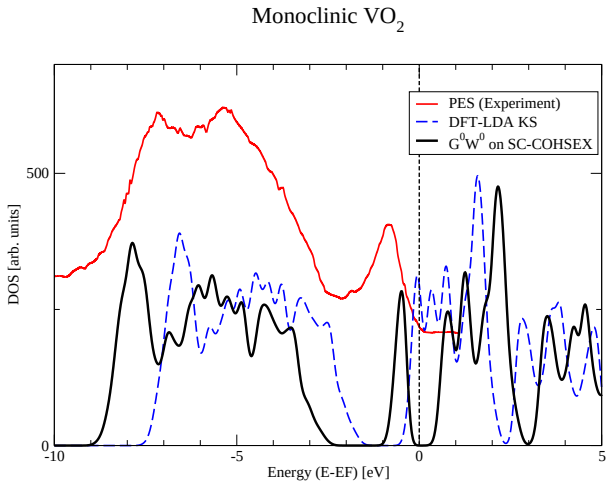

Figure 3.4: Vanadium dioxide density of states (from Ref. [Gatti 07b]). Red thin line: photoemission experiment; blue dashed line: DFT-LDA Kohn-Sham; black thick line: G^0W^0 on top of self-consistent COHSEX.

dated self-consistently, does not succeed in opening the band-gap. This points to the fact that the change of wavefunctions from LDA to QP is of the utmost importance. Indeed, analysis (see Fig. 2 of Ref. [Gatti 07b]) of the self-consistent COHSEX top-of-valence and bottom-of-conduction wavefunctions with respect to the LDA ones reveals a remix of about 10% among the d-states around the Fermi level, with an increased $d_{\|}$ character for the top-of-valence state. Notice that already the self-consistent *static* COHSEX approximation was able to open the band gap to a value, 0.78 eV, which is not far from the experimental 0.6 eV. And notice also the importance to include all relevant states within the calculation and not only the t_{2g} orbitals, as done in dynamical mean-field theory (DMFT) or cluster-DMFT calculations. Indeed, a COHSEX calculation where the self-consistency is only limited to the t_{2g} still opens the band-gap, but only to 0.36 eV.

As a final result, we have shown that our RPA result for the energy-loss function $-\Im\varepsilon^{-1}$ that enters the dynamically screening $W = \varepsilon^{-1}w$ and thus the GW self-energy, is itself in good agreement with experimental EELS spectra (Fig. 3.5) . In particular, in the rutile phase it presents a plasmon resonance at 1.3 eV which is characteristic for the metal, while in the insulator is absent. This could explain the difference in the satellite structure between the photoemission spectra of the two phases. Our *ab initio* GW calculation hence explains the peak seen in the ARPES spectral function of the metal as being a *plasmon satellite* of the main quasiparticle peak, rather than a lower Hubbard band as indicated by DMFT calculations [Biermann 05].

3.8 Beyond GW: BSE and vertex corrections

We close this chapter by providing two sections to be seen as in perspective, rather than as already accomplished tasks. Although as shown in the two pro-

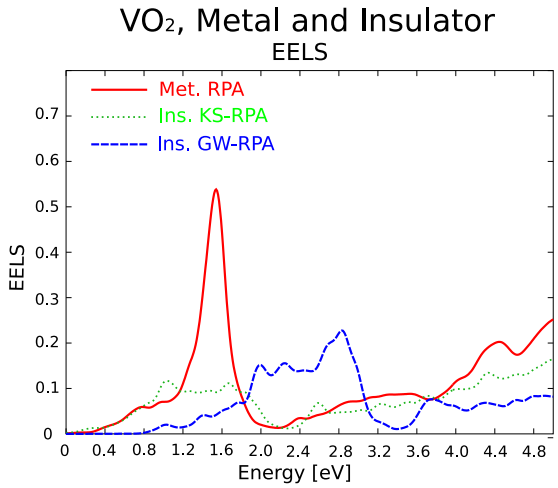

Figure 3.5: Vanadium dioxide energy-loss function $-\Im\varepsilon^{-1}(\omega)$ (from Ref. [Gatti 07b]). Solid red line: metallic rutile phase in RPA; blue dashed line: insulating monoclinic in KS-RPA; green dotted line: insulating monoclinic in GW-RPA.

vided examples and from Fig. 3.1, GW seems to be a valid approach over quite a large range of systems and applications, we must not forget that GW is an approximation to the exact result. Breakdowns of the approximation should be expected, and this will set the limits of GW. The limits of GW might be set somewhere in the strongly correlated phenomenology and strong-correlated systems. With strong-correlated systems we here mean systems where the band paradigm is not any more holding and they are presenting spectral functions where most of the spectral weight is transferred to the incoherent part, rather than being concentrated under well defined quasiparticle structures. Or also GW can surprisingly be able even to describe a strongly correlated phenomenology at least qualitatively, if not quantitatively. These are the fundamental questions to be answered in the next years by a deep study of the application of the GW approximation on strongly correlated systems, starting from transition metal oxydes. For most of them we will probably discover that the situation is not much different from what we have found in VO_2. That is, that the band paradigm could be in many cases predominant over the strongly correlated paradigm than actually believed. But the important workbench test of the GW approximation will be on systems where the strongly correlated paradigm is fully realized. In case the GW approximation will be found not working on these system, we shall be ready to go beyond the GW approximation if we want to still have an *ab initio* first principles theory without adjustable parameters.

From another point of view, we have already evidenced a limit of the GW approximation. Indeed, when we are dealing with observables related to neutral excitations and optical spectra as measured in ellipsometry rather than charged excitations and the electronic structure as measured in ARPES, the GW approximation breaks down and the results are not any more in agreement with the experiment (see Fig. (2.2). Optical spectra in semiconductors

and insulators are in many cases not even qualitatively reproduced by the GW approximation. The neglect of the vertex (i.e. $\tilde{\Gamma} = 1$) is to be considered a good approximation for the self-energy $\tilde{\Sigma}$, Eq. (3.8), but not for the polarizability $\tilde{\Pi}$, Eq. (3.8). When calculating neutral excitations and optical spectra extracted from the polarizability, we need to go beyond the GW approximation and introduce *vertex corrections*, beyond the GW approximation bare vertex expression $\tilde{\Gamma}^{\mathrm{GW}} = 1$. This can today be done by the so called *Bethe-Salpeter equation* (BSE) approach. It is a way to introduce a vertex correction in the expression for the polarizability $\tilde{\Pi}$, Eq. (3.8). In this approach, the kernel of the Bethe-Salpeter equation, equivalent to the kernel of the Hedin's vertex equation Eq. (3.8), $\Xi_{\mathrm{M}} = \delta\tilde{\Sigma}_{\mathrm{M}}/\delta G$, is approximated using its second iteration expression and considering the GW as the first iteration. That is,

$$\Xi_{\mathrm{M}} = \frac{\delta\tilde{\Sigma}_{\mathrm{M}}}{\delta G} \simeq \frac{\delta\tilde{\Sigma}_{\mathrm{M}}^{\mathrm{GW}}}{\delta G} = iW + iG\frac{\delta W}{\delta G} \simeq iW, \tag{3.8}$$

and this kernel is used to calculate the *irreducible two-particle correlation function* $\tilde{L}$ by resolution of the Bethe-Salpeter equation,

$$\tilde{L} = GG + GG\Xi_{\mathrm{M}}\tilde{L}. \tag{3.9}$$

The polarizability is then directly derived from $\tilde{L}$ by contraction of two of its indeces, $\tilde{\Pi}(x_1, x_2) = -iL(x_1, x_2, x_1^+, x_2^+)$, and from the polarizability the dielectric function and all observables. This is a way to calculate a *second iteration* polarizability $\tilde{\Pi}$ which includes some vertex corrections. The results one can get by this procedure is shown in Fig. (2.2), where the BSE curve is in good agreement with the experiment, while the GW approximation curve, neglecting vertex corrections, is not able to catch electron-hole interaction effects. The conclusion is that whenever electron-hole interaction effects have an important role, the GW approximation will be lacking. And the BSE approach can be a possible way to overcome the problem.

We would like to mention another possible route to go beyond the GW approximation we have explored in Ref. [Bruneval 05]. In this approach, we propose to develop the 2-particle effective interaction Ξ_{M} in Eq. (3.8) by functional deriving the self-energy $\tilde{\Sigma}_{\mathrm{M}}$ with respect to the *electronic density* ρ, rather than the Green's function. This leads to a simplified 3-point expression for the $\Xi_{\mathrm{M}}(x_1, x_2; x_3)$ rather than a complete 4-point, and there is hope to simplify further the expression by approximating non-local terms, likely to be small with respect to the rest. Along this way we have shown some encouraging results. This can be a promising way in order to go beyond the GW approximation in systems where it will break down.

3.9 Perspectives beyond MBQFT

Finally, excitations and spectroscopy could well be addressed by other, new theories, else than MBQFT. We have already seen TDDFT, but this theory is unsuitable for charged excitations. TDDFT is an in principle exact theory to provide the optical gap, but not the fundamental photoemission gap, the gap in the electronic band structure of the system. Although it would seem that charged excitations, such as electron addition/removal energies, would be

accessible only to a field theory where we have well defined creation and distruction operators, there are other possible ways to tackle the problem. One of them has been explored during Matteo Gatti's PhD thesis's work [Gatti 07c] and it is based on a generalization of the so-called Sham-Shlüter equation [Sham 83]. We introduce a ficticious, unphysical non-interacting system s such as the single-particle Hamiltonian seen by its electrons is $h^{(0)} + v^s$, that is the non-interacting (kinetic + external potential) Hamiltonian plus an *effective potential* v^s which can be a local and static operator $v^s(x)$. Here however we let the freedom of more degrees of freedom, toward non-locality $v^s(x_1, x_2)$ and/or dynamicity $v^s(x, \omega)$. We can then calculate the Green's function of this ficticious system $G^s = (\omega - h^{(0)} - v^s)^{-1}$, and we have a Dyson equation, $G = G^s + G^s(\tilde{\Sigma} - v^s)G$, which relates the physical quantities $\tilde{\Sigma}$, G, to the accessory ones v^s, G^s. The ancillary quantities can then be fixed by imposing that one or some observables are provided exactly by the ficticious system. For example, we can construct the auxiliary system s such as the electronic density $\rho(x) = -iG(x, x^+)$ is in principle provided exactly by G^s and the ficticious system, $\rho(x) = -i\,\mathrm{diag}[G] = -i\,\mathrm{diag}[G^s]$. This is the definition of the Kohn-Sham system. Notice that such a system is constructed such as the electronic density is provided exactly, but there is no reason why also other quantities, such as the electronic structure or the band gap, are provided exactly. From the Dyson's equation by application of the diag projector we can derive the *Sham-Schlüter equation*

$$\mathrm{diag}[G^s(\tilde{\Sigma} - v^s)G] = 0, \tag{3.10}$$

which allows to calculate the Kohn-Sham potential v^s provided we know the exact Green's function G and the exact self-energy $\tilde{\Sigma}$. One can see that a static and local $v^s(x)$ has already enough degrees of freedom to provide an exact density $\rho(x)$. Used in this way the Sham-Shlüter equation is useless. Indeed, to calculate $v^s(x)$ you need to know the exact self-energy, which corresponds to having solved the problem. But this approach can help in finding good approximations for the effective potential v^s. For instance, this is the way used in so called optimized effective potential (OEP) approaches to DFT.

Now the idea contained in Ref. [Gatti 07c] is that we can go beyond DFT KS and situate half-way from full MBQFT: we can construct the auxiliary system so that it is in principle exact to provide not only the density, but also the total spectral function $A(\omega) = -\pi^{-1}\Im G(\omega)$, which is related to the trace in reciprocal or real space of the imaginary part of the Green's function with its full frequency dependence. Indeed, from the total non angle-resolved spectral function one can read the fundamental (indirect) band-gap of the system and conclude whether the system is a metal or an insulator. The condition to be asked is hence that $\Im G(r, r, \omega) = \Im G^s(r, r, \omega)$, and this will set the associated effective potential v^s. One important conclusion shown by our work [Gatti 07c] is that an effective local potential $v^s(r)$ has not enough degrees of freedom to allow the ficticious system to reproduce exactly both the density and the total spectral function. A local $v^s(r)$ can only reproduce the exact density, and there is no possibility that it can also reproduce the band-gap. This is the reason why an ordinary DFT Kohn-Sham approach, with a local Kohn-Sham potential, cannot in principle reproduce the exact band-gap of a system. Looking for approximations of the Kohn-Sham potential beyond the LDA or GGA, can produce better results on the band-gap of a given class of systems, but it cannot be systematic.

On the other hands, we can go beyond DFT and KS toward an intermediate theory, between DFT and MBQFT, with an effective potential which is for example dynamic, $v^s(r,\omega)$ (or non-local $v^s(r_1,r_2)$, since we have shown that the two are equivalent, one can be reduced to the others). And thank to this complication, still simpler than the full self-energy $\tilde{\Sigma}(r_1,r_2,\omega)$, we can address the electronic density and at the same time the band-gap problem. The resulting effective theory is less complex than full MBQFT and is in principle correct way to tackle the band-gap problem. I think that such approaches can have a future in our domain. Provided we are able to find good approximations within the new theory, as LDA or GGA are good approximations for ordinary DFT and the Kohn-Sham system.

Chapter 4

Quantum transport by NEGF

Many-body *e-e* scattering effects are also important when dealing with the problem of quantum transport. Electronic quantum transport [Datta 95, Di Ventra 08] is the field of physics that studies the conductance in electronic devices at the mesoscopic and, more recently, nanoscopic scale. In fact *nanoelectronics* represents the next years' technological challenge, boosted not only by the need for shorter integration scales, but also by the expectation that unusual quantum effects are going to be observed due to quantum phenomena effects. Beside the experimental efforts to synthesize nanoelectronic devices, the theory of quantum transport has the formidable task to understand and to model the mechanisms behind these phenomena, and at last to predict them from first principles by an *ab initio* approach.

In this chapter we briefly introduce the very fundamentals of non-equilibrium Green's function (NEGF) theory [Kadanoff 62, Haug 96], which is an in principle exact framework to address quantum transport. NEGF is a theory beyond the state-of-the-art Landauer formalism applied on top of tight-binding or also density-functional theory and much more appropriated than Landauer on top of DFT. Indeed, NEGF can provide the exact electronic structure of the system, keeping correctly into account many-body *e-e* and *e-ph* interaction effects. Further, it is a truly out-of-equilibrium theory, which is the situation to be accounted in quantum transport when applying a finite bias across the system. NEGF can also describe the open-system situation of the *principal layers* quantum transport workbench, whish is the most used framework to tackle the problem. In the last section, we describe also recent developments that led us to the definition of a new quantum transport workbench, beyond the principal layers and presenting some numerical and physical advantages with respect to the latter.

All these developments have been carried out during the last 4 years thank to Pierre Darancet and his PhD thesis work [Darancet 08], which have been co-supervised by Didier Mayou and myself.

4.1 Non-equilibrium Green's function theory

Non-equilibrium quantum field theory or non-equilibrium Green's function (NEGF) theory is an extension of finite-temperature MBQFT that can describe the system even when out of equilibrium. That is the normal situation in quantum transport where a finite bias/potential difference is applied to make current flow in the conductor. In NEGF, the full Hamiltonian Eq. (3.1) is extended to be

$$\hat{\mathcal{H}} = \hat{H} + \hat{U}(t) = \hat{H}^{(0)} + \hat{W} + \hat{U}(t) = \hat{T} + \hat{V} + \hat{W} + \hat{U}(t) \tag{4.1}$$
$$\hat{U}_S(t) = \int dr_1 dr_2\, u(r_1, r_2, t)\hat{\psi}_S^\dagger(r)\hat{\psi}_S(r) \qquad u(r_1, r_2, t) = 0 \quad \forall t < t_0$$

where $\hat{U}_S(t)$ (in the Schrödinger picture) is a time-dependent external potential term representing the applied bias. It is switched on at $t = t_0$ and drives the system out-of-equilibrium. This term introduces a further complication, beyond the problem represented by the many-body term $\hat{W}$. NEGF is a very complete framework which allows to deal with:

1. The many-body description of *incoherent transport*, thus including *e-ph* and *e-e* interactions and electronic correlations;
2. The *out-of-equilibrium* situation;
3. The *transient response*, beyond the steady-state;
4. It reduces to the Landauer formalism in the coherent regime.

Formulation of the theory starts from writing the expression for time-dependent observables, average values of quantum operators. In finite-temperature MBQFT (we take back the case with $\hat{U}(t) = 0$), an observable is given by the average value of the corresponding quantum operator over the ground and excited states weighted by the corresponding statistical weight. In the canonical ensemble, this is written as

$$\bar{o} = \sum_i \frac{e^{-\beta E_i}}{Z}\langle\Psi_i|\hat{o}|\Psi_i\rangle = \mathrm{tr}[\varrho(\hat{H})\hat{o}_H(t)], \tag{4.2}$$

where $\varrho(\hat{H}) = e^{-\beta\hat{H}}/Z$ is the canonical statistical weight and $Z = \mathrm{tr}[e^{-\beta\hat{H}}]$ the partition function. The expression can eventually be generalized to the grand-canonical ensemble with $\varrho(\hat{H}, \hat{N}) = e^{-\beta(\hat{H}-\mu\hat{N})}/\mathcal{Z}$, and $\mathcal{Z} = \mathrm{tr}[e^{-\beta(\hat{H}-\mu\hat{N})}]$ the grand-partition function. $\hat{o}_H(t)$ is written in the Heisenberg picture with respect to the Hamiltonian $\hat{H}$. Of course, in the 0-temperature case ($\beta \to \infty$), the weight ϱ is such that only the ground state provides a contribution to the observable and we get the traditional expression $\bar{o} = \langle\Psi_0|\hat{o}|\Psi_0\rangle$. Now let's consider the full Hamiltonian $\hat{\mathcal{H}}$ and switch on the time-dependent external source $\hat{U}(t)$ which, starting from $t = t_0$, drives the system out of equilibrium. We can write a generical observable as

$$\bar{o}(t) = \mathrm{tr}[\varrho(\hat{H})\hat{o}_{\mathcal{H}}(t)],$$

where the operator $\hat{o}_{\mathcal{H}}(t)$ is in the Heisenberg picture ($_{\mathcal{H}}$) with respect to the full Hamiltonian $\mathcal{H}$ and the statistical weigth is referred to the unperturbed

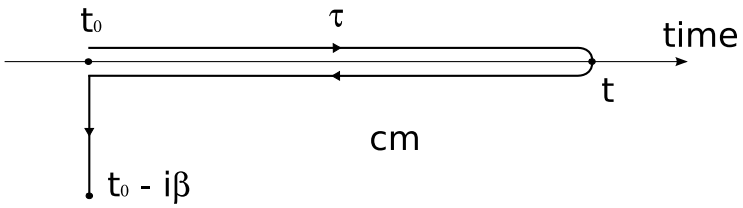

Figure 4.1: Schwinger-Keldysh contour.

hamiltonian $\hat{H}$ and the equilibrium situation before t_0. It can be demonstrated that the average value can be written in the form

$$\bar{o}(t) = \frac{1}{Z}\,\mathrm{tr}\left[T_c\left\{e^{-i\int_c d\tau\,\hat{U}_H(\tau)}\hat{o}_H(t)\right\}\right] \tag{4.3}$$

where everything is in the Dirac or interaction (with respect to U) representation $(_H)$, corresponding to the Heisenberg representation for the unperturbed Hamiltonian $\hat{H}$, and we define the operators on times τ over the Schwinger-Keldysh [Schwinger 61, Keldysh 64] contour c shown in Fig. 4.1, over which it is also defined the contour-ordered operator T_c. This can be seen as a trick to take into account, within a single expression, both the time-evolution in presence of a time-dependent Hamiltonian and the statistical weight ϱ, which is accounted by the Matsubara section of the Keldysh contour, that is an evolution along imaginary time up to $-i\beta$.

Every observable can be conveniently represented in the form Eq. (4.3) and so also the Green's function. We can introduce a contour-time ordered $T_c\{\hat{o}(t_1)\hat{p}(t_2)\}$ product which reverts the order of the operators (and changes the sign for fermions) whenever $t_2 >_c t_1$ *along the contour* coordinate τ. The *contour-ordered* Green's function G^{co} is hence defined

$$G^{co}(x_1, x_2) \stackrel{def}{=} \overline{(-i)T_c\{\psi_{\mathcal{H}}(x_1)\psi^{\dagger}_{\mathcal{H}}(x_2)\}}. \tag{4.4}$$

By this definition of the Green's function on the contour we can recover Wick's theorem and hence perturbation theory, exactly as in 0 and finite temperature MBQFT. The contour-ordered Green's function G^{co} is equal to one of the four ordinary (anti)-time-ordered Green's function G^{to}, G^{ato}, or the correlation functions $G^{<}$ or $G^{>}$, depending on which branch of the ficticious contour, $c_{\rightarrow}$ or $c_{\leftarrow}$, the physical time coordinates t_1 and t_2 are placed. We then have:

$$G^{co}(x_1, x_2) = \begin{cases} G^{to}(x_1, x_2) & t_1, t_2 \in c_{\rightarrow} \\ G^{>}(x_1, x_2) & t_1 \in c_{\leftarrow}, t_2 \in c_{\rightarrow} \\ G^{<}(x_1, x_2) & t_1 \in c_{\rightarrow}, t_2 \in c_{\leftarrow} \\ G^{ato}(x_1, x_2) & t_1, t_2 \in c_{\leftarrow} \end{cases}$$

In NEGF it is not any more sufficient to calculate only one Green's function, for example the time-ordered G^{to} like in 0 or finite temperature MBQFT. In the most general case we need to calculate three independent quantities among those indicated above (the forth can be calculated as combination of the others). For example, we can choose the time-ordered G^{to} (or better the retarded Green's function G^{r}) plus the correlation functions $G^{<}$ and $G^{>}$. The latter have the

physical meaning of distribution functions for electrons and holes, respectively. At equilibrium, of course, only one is linear independent, and we can for example write

$$-iG^{<} = f_{\mathrm{FD}}(\omega)A(\omega)$$
$$+iG^{>} = [1 - f_{\mathrm{FD}}(\omega)]A(\omega)$$

that is, the correlations functions are recovered by the spectral function (and thus $\Im G^{to}$) and the equilibrium Fermi-Dirac distribution functions. This is not any more true out of equilibrium.

We can now write the fundamental equation of motions of NEGF for the three independent quantities:

$$\begin{aligned} G^r &= [\omega - h^{(0)} - \Sigma^r]^{-1} \\ G^{<} &= G^r \Sigma^{<} G^a \\ G^{>} &= G^r \Sigma^{>} G^a \end{aligned} \tag{4.5}$$

that are valid only at the steady-state. The first equation is the ordinary Dyson equation relying the Green's function and the self-energy (here written for the causal retarded quantities). In the last two equations (the equations of motion for the correlation functions) we have introduced the *scattering functions* $\Sigma^{<}$ and $\Sigma^{>}$, physically representing the rates at which electrons and holes scatter in and out a given energy and momentum. Combination of the two gives the decay rate Γ (not to be confused with the vertex function)

$$\Gamma = i[\Sigma^{>} - \Sigma^{<}] = i[\Sigma^r - \Sigma^a] \tag{4.6}$$

at a certain energy and momentum. Again, at equilibrium

$$-i\Sigma^{<} = f_{\mathrm{FD}}(\omega)\Gamma(\omega) \tag{4.7}$$
$$+i\Sigma^{>} = [1 - f_{\mathrm{FD}}(\omega)]\Gamma(\omega) \tag{4.8}$$

and there is no need to introduce the scattering functions, since the self-energy is a sufficient degree of freedom for the system. Self-energy and scattering functions contain the effect of the many-body *e-e* as well as the *e-ph* interactions. We will see in the next paragraph the composition of the self-energy in a quantum transport system.

4.2 The principal layers workbench

To tackle the quantum transport problem the first step is to introduce a "workbench" model which we assume to be representative of the system to be studied. In NEGF and also in the Landauer formalism, the most used workbench is the so-called *principal layers* (PL) workbench (Fig. 4.2 top). In PL the quantum transport system is separated into 3 parts: a central C "extended molecule" region, including the molecule or the nanodevice we are studying plus some layers in reality belonging to the leads. This to keep into account relaxation of the electronic structure at the contact. Then there are two external regions, the left L and right R leads, which we suppose seminfinite and periodic. Within this workbench the focus is on the central region, with the effects of the external

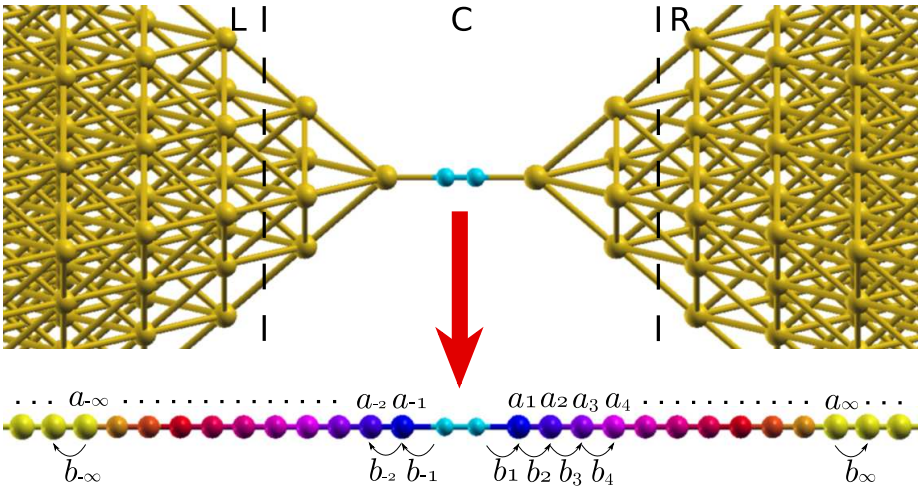

Figure 4.2: Principal layers workbench model (top scheme). It is characterized by a central C "extended molecule" (here H_2) region (including part of the leads) and the left L and right R leads (here gold) regions. Bottom: mapping of the real 3D device onto the *effective 1D system* (the effective atomic chain at the bottom). The *effective channels* arise from the central device (here the hydrogen molecule) and pursue into a non-ballistic section (blue, violet and red pseudoatoms), until they achieve an asymptotic ballistic behaviour (yellow).

leads taken into account by *leads self-energies* (together with the corresponding scattering functions) Σ_L and Σ_R. These can be calculated from the Green's functions $g_{L,R}$ of the leads and the coupling Hamiltonian H_{LC} and H_{CR} between the leads and the central region,

$$\begin{aligned} \Sigma_L &= H_{CL} g_L H_{LC} & \Sigma_R &= H_{CR} g_R H_{RC} \\ g_L &= (\omega - H_L)^{-1} & g_R &= (\omega - H_R)^{-1} \end{aligned}$$

In the PL the leads are assumed at equilibrium, each one with its chemical potential μ_L and μ_R and with their scattering functions given by the equilibrium expressions Eqs. (4.7, 4.8). They are also assumed ballistic, in the sense there are no scattering processes, *e-e* or else, within the leads.

The total self-energy and scattering functions acting on the central region result from the sum of the leads self-energies and the *e-e* and *e-ph* self-energies,

$$\Sigma^{r<>} = \Sigma^{r<>}_{e\text{-}e} + \Sigma^{r<>}_{e\text{-}ph} + \sum_{T=L,R} \Sigma^{r<>}_{T},$$

and the Green's function for the central region is given by the NEGF equations of motion Eq. (4.5). Once solved the equations and got G for the central C region, the current flowing from a terminal $T = L$ or R is calculated by the Meir-Wingreen formula

$$i_T = \frac{e}{h} \mathrm{tr}[\Sigma^{<}_T G^{>} - \Sigma^{>}_T G^{<}]. \tag{4.9}$$

It can be shown that in the case of coherent transport, that is when both *e-e* and *e-ph* interaction effects are switched off together with their self-energies, the Meir-Wingreen formula reduces to the Fisher-Lee formula

$$C = \frac{2e^2}{h} \, \mathrm{tr}[\Gamma_L G^r \Gamma_R G^a], \tag{4.10}$$

where C is the conductance of the system. In this limit NEGF reduces to the ordinary Landauer formalism with an electronic structure calculated at the level of the independent-particle, non-interacting Hamiltonian $h^{(0)}$. In the "Landauer on top of DFT" approach, the latter is replaced by the Kohn-Sham Hamiltonian h^{KS}, in the hope to somehow include some exchange and correlation effects.

4.3 GW-NEGF

In the last years, combination of an electronic structure calculated at the level of *ab initio* DFT together with the description of transport properties in a Landauer framework, has demonstrated its ability to describe small bias coherent transport in nanojunctions. These approaches were successful in accounting for the contact resistance and conductance degrading mechanisms induced by impurities, defects and non-commensurability patterns in the conductor region. The major objections raised to this approach are:

1. The use of the in principle unphysical Kohn-Sham electronic structure has to be considered only as an approximation to the true quasiparticle electronic structure;

2. Non-coherent and dissipative effects due to electron-phonon (*e-ph*) and electron-electron (*e-e*) scattering can be taken into account only approximatively in the Landauer formalism;

3. Non-linear response and far from equilibrium finite-bias transport are not accessible, since DFT cannot be applied to open systems and it is not a non-equilibrium theory.

NEGF is in principle a correct framework to tackle the above objections. This is the reason why we decided to address to this theory. The critical point within this theory is the choice of good approximations to the self-energy Σ^r, and coherently to the scattering functions $\Sigma^{<,>}$. This ensures that both the renormalization of the QP energies and the electron diffusion mechanisms due *e.g.* to *e-ph* or *e-e* interactions, will be properly taken into account. A first work studying the role of a *e-ph* self-energy in the self-consistent Born approximation (SCBA) appeared in literature [Frederiksen 04]. The work studied a very simple but real system, a gold monoatomic chain, where a reliable experiment was available [Agraït 02]. During Pierre Darancet's thesis work we decided to study the role of electronic correlations on the same system. The purpose was to evaluate the effect of *e-e* interaction with respect to the previously studied *e-ph*, whether of the same order or else, and to compare both to the experiment. Electronic correlations were introduced in the calculation of transport by an *ab initio* approach based on the GW approximation in the framework of NEGF. To do it properly, one should resort a fully non-equilibrium GW approximation

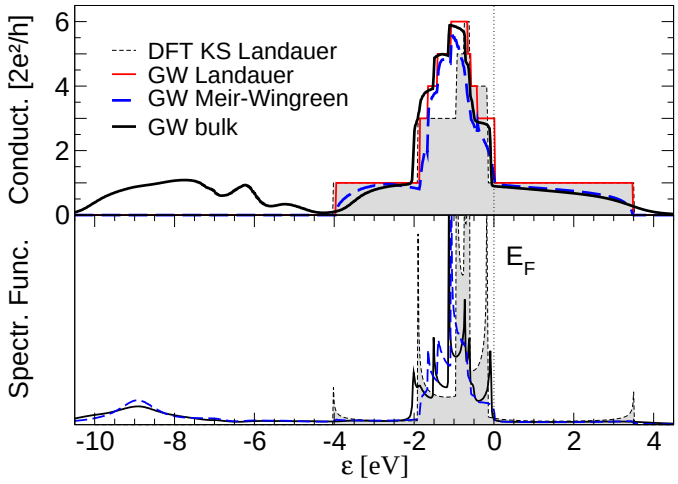

Figure 4.3: Conductance (top) and spectral function (bottom) for a gold monoatomic chain (reproducing Fig. 3 of Ref. [Darancet 07]). Thin dashed line: Landauer result using a DFT KS structure; thin solid line: Landauer using only a real part GW renormalization of the energies; thick dashed line: Meir-Wingreen result using GW real part renormalization in the leads and a full (hermitean+anti-hermitean) dynamical GW self-energy in the conductor; thick solid line: GW bulk conductance with full dynamical self-energy.

as done in Ref. [Spataru 04]. In our scheme however [Darancet 07], since we wanted to study as in Refs. [Frederiksen 04, Agraït 02] the nearly equilibrium transport at a bias of few tens of meV, the GW self-energy is built at equilibrium and the Green's function is calculated by direct solution of the Dyson equation. For the lead/conductor/lead geometry, the GW self-energy is summed to the lead's self-energies. The electronic conductance is calculated through a modified Meir-Wingreen formula [Meir 92] re-derived by Ref. [Ferretti 05] under more general conditions. This is a NEGF Landauer-like expression valid for interacting conductors at equilibrium. We apply this scheme to the gold mono-atomic onedimensional chain and we study the effects induced on transport properties by the different components of the GW self-energy, the hermitean and the non-hermitean parts and the dynamical dependence. We study the bulk conductance and we also artificially partition the system into three regions: the right and left leads – two semi-infinite gold mono-atomic chains – and a central region, constituted by a single gold atom. This has the purpose to clarify the role of both intra-conductor and conductor-lead correlations.

In Fig. 4.3 we show the conductance and the spectral function of the gold chain obtained using different methods: The black thin dashed line is calculated using the Landauer formula and the DFT KS electronic structure. The conductance at the Fermi level appears to be one (in units of $2e^2/h$) and it is of s-like character. The red thin solid line is obtained from the Landauer formula evaluated using the GW real-part-only QP energies. GW corrections are considered both in the conductor and in the leads. Otherwise, a ficticious contact resistance, unphysical for a homogeneous system, would appear. At

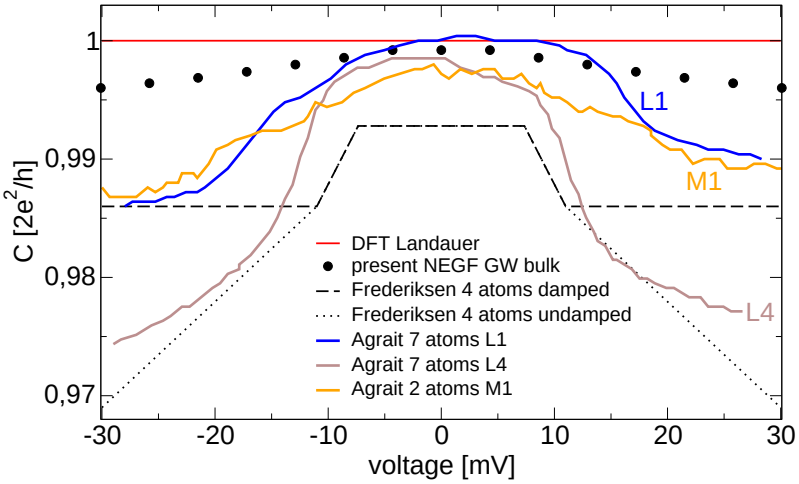

Figure 4.4: Differential conductance vs applied bias (reproducing Fig. 4 of Ref. [Darancet 07]). Thin solid line: DFT Landauer result; dots: NEGF GW bulk result; dashed and dotted line: *e-ph* theory of Ref. [Frederiksen 04] corresponding to 4 atoms, same interatomic distance and for the damped and undamped limits; thick solid lines: experimental result of Ref. [Agraït 02] corresponding to 2 and 7 atoms and different chain strains.

this first level, the net effect is a renormalization of KS into QP energies, the true energies to introduce and remove an electron from the system. Therefore, the conductance profile is considerably modified by the real part of the GW correction. The position of the conductance steps is especially modified in the *d*-like region (~ -1 eV). The blue thick dashed line represents the result obtained in the tri-partitioned geometry by using the Meir-Wingreen formula and introducing a full non-hermitean and dynamical GW self-energy in the conductor. Static real-part-only QP energies are included in the leads. This introduces loss-of-coherence only in the conductor, while leaving the leads ballistic. At the same time it limits the introduction of ficticious contact resistances, *i.e.* the QP levels are aligned in the leads and the conductor. The difference of this curve with respect to the thin solid line genuinely represents the effect of *e-e* scattering mechanisms in the conductor, causing diffusion, loss of coherence and appearance of resistance. Thus the imaginary part of the GW corrections introduces a suppression of the conductance, which is negligible close to the Fermi energy, but that increases with energy. The scattering of electrons due to the *e-e* interaction leads to degradation of the conductance. With respect to Landauer approaches, the spectral function now appears as a collection of broadened QP peaks, whose finite width is directly associated to the inverse of the electronic lifetime of the QP state. The spectral weight, which is spread out, results in a lowering and a spill-out of the conductance step-like profile. This effect is directly related to the imaginary part of the QP energies, and can be seen to increase with $\epsilon - E_{\mathrm{F}}$. Finally, we calculate the fully correlated bulk GW conductance by taking into account a non-hermitian and dynamical GW self-energy everywhere in the system, conductor and leads (thick solid line).

With respect to the previous case, even residual contact resistances (due to the fact that the conductor and leads spectral peaks were differently shaped, with finite and infinitesimal widths respectively) are completely removed, and the conductance increases almost overall. Only around -3 eV we see a slight drop, which we verified due to an unfavourable ratio $(\Gamma_L + \Gamma_R)^{-1}\Gamma$ between leads injection rate and total (plus correlation) one. Moreover, new structures appear in the conductance at the lowest energies. By inspecting the spectral function, we can attribute them to the presence of satellites of electronic origin, *i.e.* plasmons or shake-ups, of the main QP peaks. Since the *e-e* interaction is an elastic scattering mechanism, these satellites are necessary to balance the losses which occur at energies close to the Fermi level, and are therefore important for transport. The *e-e* scattering acts in a way to redistribute the conductance channels to different energies, rather than globally destroy conductance as in the *e-ph* scattering, where momentum and current is lost toward ionic degrees of freedom.

In Fig. 4.4 we show the voltage characteristics in the small voltage range of ± 30 mV for the gold monoatomic chain. We compare our GW results (dots) with the experimental results of Ref. [Agraït 02] (thick coloured lines) and the *e-ph* result of Ref. [Frederiksen 04] (thin black lines), calculated at exactly the same atomic geometry and at equilibrium as us. The results from Ref. [Frederiksen 04] attribute the step in the conductance, occurring at $\sim$ 15 mV, to the onset of phononic processes. Instead, the continuous drop observed in our electronic correlated conductance, occurring in the first 15 mV, compares favorably with the drop observed experimentally [Agraït 02]: *e-e* scattering mechanisms seem hence responsible for a continous drop in the conductance, especially visible at very low bias. While the quantitative agreement with the experiment on the conductance value may be somewhat fortuitous, the trend in this drop is a direct consequence of the increase in the GW imaginary part of QP energies and it is very general.

4.4 Generalized Fisher-Lee and Meir-Wingreen

Among the last developments to which, together with Didier Mayou and Pierre Darancet, we contributed in this field, there is a new quantum transport formalism which goes beyond the principal layer workbench. One may notice that in the PL (Fig. 4.2 top) the separation between the central region and the ballistic leads appears somehow arbitrary and unphysical. Indeed, in order to correctly describe the contact resistance, the central region should contain not only the conductor under study (e.g. a molecule or a nanodevice), but also some layers in reality belonging to the leads. Convergence should be checked by increasing the central region size and thus the number of states in the problem. Its computational resolution is heavier, since it deals with a number of channels much greater than the true channels of the central device. Furthermore, the natural physical separation between the leads and the true real device is lost, and a direct comprehension of resistance mechanisms is difficult.

In Ref. [Darancet 09b] we introduce a new formalism based on a map of the real 3-dimensional lead-conductor-lead system onto an *effective 1-dimensional system* (see Fig. 4.2 bottom). Central to this mapping is the notion of *effective channels* as the states through which the current flows up to the central

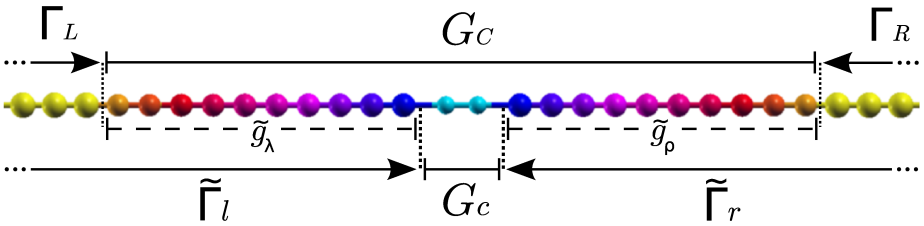

Figure 4.5: The conductance can be calculated by the traditional Fisher-Lee or Meir-Wingreen formulas and 3-partitioned workbench, with ballistic leads L and R, and extended (molecule + non-ballistic leads) central region C (scheme above); or the generalized Fisher-Lee or Meir-Wingreen formulas and the 5-partitioned workbench, with central device c, non ballistic section λ and ρ, and finally ballistic sections L and R of the effective channels (scheme below).

device. The number of these channels is bounded by the number of states of the central bottleneck. All the leads' states orthogonal to the states of the effective channels do not effectively participate to the conductance and can be safely disregarded. This is a considerable simplification with respect to the PL. The effective channels can be viewed as associated to an *effective 1-dimensional system* onto which the real 3-dimensional physical system is mapped (Fig. 4.2). This is a way to restore the natural dimensionality of the quantum transport problem, which is truly 1D. The resulting 1D effective theory is an in principle exact formalism to calculate the conductance. In practice we are going to build an orthonormal basis set $\{\psi_n\}$ for the 1D effective system. Let's first build the right effective channel space and its basis set $\{\psi_n\}$. We start from a state localized ϕ_c localized in the central bottleneck and we apply the c-r coupling Hamiltonian H_{rc} and then the right Hamiltonian H_r. The first element ψ_1 of the basis is given by $b_1|\psi_1\rangle = H_{rc}|\phi_c\rangle$. b_1 is chosen as normalization factor for ψ_1. Next we calculate $a_1 = \langle\psi_1|H_r|\psi_1\rangle$. We then calculate the second element by $b_2|\psi_2\rangle = H_r|\psi_1\rangle - a_1|\psi_1\rangle$. ψ_2 is orthogonal to ψ_1 and normalized by b_2. At the next and all the following steps we iterate the same procedure, $a_n = \langle\psi_n|H_r|\psi_n\rangle$ and $b_{n+1}|\psi_{n+1}\rangle = H_r|\psi_n\rangle - a_n|\psi_n\rangle - b_n^*|\psi_{n-1}\rangle$. This is an implementation of the standard Haydock recursion method,

$$H_r|\psi_n\rangle = a_n|\psi_n\rangle + b_n^*|\psi_{n-1}\rangle + b_{n+1}|\psi_{n+1}\rangle. \tag{4.11}$$

In conclusion, we end with an orthonormal basis $\{\psi_n\}$ for $\mathcal{S}_r^{eff}$. With increasing n, the state ψ_n is a linear combination of real orbitals belonging to atoms deeper and deeper in the contact. The recursion can be stopped at an $n = N$ where the coefficients a_n, b_n saturate and converge to an asymptotic regime, a_∞, b_∞. From this point on the leads are consequently ballistic and associated to states achieving a *maximum spread* into the contact region. On this basis set the Hamiltonian is tridiagonal, with onsite $H_{nn}^{eff} = a_n$ and (only) first neighbours hopping coefficients $H_{n,n-1}^{eff} = b_n$. It can be seen as associated to an effective 1D pseudoatomic chain (Fig. 4.5). H^{eff} is in fact the same original Hamiltonian but represented on an orthonormal basis where it is tridiagonal. The recursion basis turns out hence to be an optimal basis set, specific for quantum transport, where it is numerically very efficient.

Moreover this approach naturally leads to a physically more intuitive *5-partitioned* (instead of 3-) quantum transport workbench model (Fig 4.5 bottom scheme). This is composed by the true central conductor device, the left and right sections of non ballistic leads — which contain and isolate contact resistance mechanisms — and finally the ballistic semi-infinite leads. For this workbench we can derive a *generalized Fisher-Lee formula* to be associated to the 5-partitioned workbench,

$$C = \frac{2e^2}{h}\,\mathrm{tr}[\tilde{\Gamma}_l G_c^r \tilde{\Gamma}_r G_c^a] \tag{4.12}$$

$$\tilde{\Gamma}_l = H_{cl}\tilde{g}_\lambda^a \Gamma_L \tilde{g}_\lambda^r H_{lc}$$

$$\tilde{\Gamma}_r = H_{cr}\tilde{g}_\rho^r \Gamma_R \tilde{g}_\rho^a H_{rc} \tag{4.13}$$

This formula has a Fisher-Lee like form Eq. (4.10). But it now refers to a workbench where the Green's function G_C of the extended central region is replaced by the more significative Green's function G_c of the true device under study. The injection rates $\Gamma_{L/R}$ of ballistic leads are replaced by renormalized injection rates $\tilde{\Gamma}_{l/r}$ which refer to both the ballistic L/R and the non ballistic λ/ρ sections of the leads. In the principal layers approach all resistance mechanisms are localized within the extended central region C and considered in G_C. Here contact resistance is separated from other mechanisms, localized in the non-ballistic sections λ and ρ and transferred into $\tilde{\Gamma}$ where it is taken into account via $\tilde{g}$. The contact resistance can be read directly from $\tilde{\Gamma}$. For example, if $\tilde{\Gamma}(E) = 0$ at a given E, this will provide 0 conductance whether or not there is at E an available channel in the central device. Therefore the generalized Fisher-Lee formula allows a more clear interpretation of resistance mechanisms. Notice that the $\tilde{\Gamma}_{l/r}$ depend only on the electronic structure of the contact and on its coupling to the central device.

The 5-partitioned workbench is particularly convenient in the case of correlated transport within NEGF. Starting from the Meir-Wingreen formula Eq. (4.9) for the current, the non-coherent term can be separated from the coherent. For the coherent term we end again to the generalized Fisher-Lee Eq. (4.12). For the non-coherent current we can derive a generalized Meir-Wingreen expression of the form:

$$i_t^{\mathrm{noncoh}} = \frac{e}{h}\,\mathrm{tr}[\tilde{\Sigma}_t^{<} G_c^r \Sigma_{corr}^{>} G_c^a - \tilde{\Sigma}_t^{>} G_c^r \Sigma_{corr}^{<} G_c^a], \tag{4.14}$$

where $\Sigma_{corr}^{<>}$ are the in/out scattering functions related only to correlations (*e-e* or *e-ph*), while $\tilde{\Sigma}_t^{<>}$ are the in/out renormalized lead t scattering functions, $\tilde{\Sigma}_t(z) = H_{ct}\tilde{g}_\tau^a(z)\Sigma_T(z)\tilde{g}_\tau^r(z)H_{tc}$, where $\Sigma_T(z)$ is calculated in the ballistic region. Contact resistance is now physically separated into $\tilde{\Sigma}_t$ with respect to the resistance raising from *e-e* and *e-ph* scattering mechanisms, associated and localized into the true central device and G_c. This more faithfully represents the workbench ideal assumption of lost-of-coherence effects only within the true central device, with leads assumed as everywhere perfectly coherent. This approach has been succesfully applied to graphene ribbons in Ref. [Darancet 09a].

4.5 Perspectives

Quantum transport is a domain where there is a huge gap between the experiment and theory. For instance, for systems like organic molecules between metallic leads, the DFT plus Landauer approach provides even at 0 bias (i.e. at equilibrium) conductances which are up to 3 orders of magnitude larger than the experiment. The role of correlations could be crucial in bridging this gap, apart from being central in explaining *e.g.* Coulomb blockade and Kondo effects. This is the reason why we started a GW-NEGF 0-bias conductance study on benzene dithiol in between gold leads, a prototype system within that class and for which quite reliable experiments exist. This is a work started here during the Post-Doc of Paolo Emilio Trevisanutto and now carried on in collaboration with the Université Catholique de Lovain, with in particular many efforts by Tonatiuh Rangel, PhD student under the supervision of Gian-Marco Rignanese.

Further perspectives into this field point toward a truly beyond-equilibrium approach within GW-NEGF. In principle this would require to achieve also self-consistence in the recalculation of the GW self-energy. However there is hope that a first iteration after the calculation of the non-equilbrium distribution functions will be enough to provide reasonable results. This is however a project requiring much work, possibly in a coordinated effort within an european network.

Bibliography

[Adler 62] S. L. Adler. Phys. Rev., vol. 126, page 413, 1962.

[Adragna 01] G. Adragna. PhD thesis, Università di Roma "Tor Vergata", Rome, March 2001.

[Adragna 03] G. Adragna, R. Del Sole & A. Marini. *Ab initio calculation of the exchange-correlation kernel in extended systems.* Phys. Rev. B, vol. 68, page 165108, 2003.

[Agraït 02] N. Agraït, C. Untiedt, G. Rubio-Bollinger & S. Vieira. Phys. Rev. Lett., vol. 88, page 216803, 2002.

[Albrecht 98] S. Albrecht, L. Reining, R. Del Sole & G. Onida. Phys. Rev. Lett., vol. 80, page 4510, 1998.

[Ashcroft 76] N. W. Ashcroft & N. D. Mermin. Solid state physics. Philadelphia, 1976.

[Battistoni 96] C. Battistoni, E. Bemporad, A. Galdikas, S. Kaciulis, G. Mattogno, S. Mickevicius & V. Olevano. Appl. Surf. Sci., vol. 103, page 107, 1996.

[Biermann 05] S. Biermann, A. Poteryaev, A. I. Lichtenstein & A. Georges. Phys. Rev. Lett., vol. 94, page 026404, 2005.

[Bostwick 07] A. Bostwick, T. Ohta, T. Seyller, K. Horn & E. Rotenberg. Nature Physics, vol. 3, page 36, 2007.

[Botti 04] S. Botti, F. Sottile, N. Vast, V. Olevano, H. C. Weissker L. Reining, A. Rubio, G. Onida, R. Del Sole & R. W. Godby. *Long-Range Contribution to the Exchange-Correlation Kernel of Time-Dependent Density-Functional Theory.* Phys. Rev. B, vol. 69, page 155112, 2004.

[Botti 05] S. Botti, A. Fourreau, F. Nguyen, Y.-O. Renault, F. Sottile & L. Reining. Phys. Rev. B, vol. 72, page 125203, 2005.

[Brihuega 08] I. Brihuega, P. Mallet, C. Bena, S. Bose, C. Michaelis, L. Vitali, F. Varchon, L. Magaud, K. Kern & J. Y. Veuillen. Phys. Rev. Lett., vol. 101, page 206802, 2008.

[Bruneval 05] F. Bruneval, F. Sottile, V. Olevano, R. Del Sole & L. Reining. *Many-body perturbation theory using the density-functional concept: beyond the GW approximation.* Phys. Rev. Lett., vol. 94, page 186402, 2005.

[Calandra 07] M. Calandra & F. Mauri. Phys. Rev. B, vol. 76, page 205411, 2007.

[Darancet 07] P. Darancet, A. Ferretti, D. Mayou & V. Olevano. *Ab initio GW electron-electron interaction effects in quantum transport.* Phys. Rev. B, vol. 75, page 075102, 2007.

[Darancet 08] P. Darancet. *Theory and numerical simulation of quantum transport in nanostructures.* PhD thesis, Université Joseph Fourier, Grenoble, December 2008.

[Darancet 09a] P. Darancet, V. Olevano & D. Mayou. *Coherent electronic transport through graphene constrictions: subwavelength regime and optical analogy.* Phys. Rev. Lett., vol. 102, page 136803, 2009.

[Darancet 09b] P. Darancet, V. Olevano & D. Mayou. *Effective one-dimensional theory and generalized Fisher-Lee formula for quantum transport at nanocontacts.* cond-mat, no. 0903.0854, 4 Mar 2009.

[Datta 95] S. Datta. Electronic transport in mesoscopic systems. Cambridge University, New York, 1995.

[Del Sole 03] R. Del Sole, G. Adragna, V. Olevano & L. Reining. *Long-range behavior and frequency dependence of exchange-correlation kernels in solids.* Phys. Rev. B, vol. 67, page 045207, 2003.

[Di Ventra 08] M. Di Ventra. Electronic transport in nanoscale systems. Cambridge University, Cambridge, 2008.

[Eyert 02] V. Eyert. Ann. Phys., vol. 11, page 650, 2002.

[Ferretti 05] A. Ferretti, A. Calzolari, R. Di Felice & F. Manghi. *First-principles theoretical description of electronic transport including electron-electron correlation.* Phys. Rev. B, vol. 72, page 125114, 2005.

[Fetter 71] A. L. Fetter & J. D. Walecka. Quantum theory of many-particle systems. McGraw-Hill, New York, 1971.

[Frederiksen 04] T. Frederiksen, M. Brandbyge, N. Lorente & A. P. Jauho. Phys. Rev. Lett., vol. 93, page 256601, 2004.

[Galdikas 97] A. Galdikas, V. Jasutis, S. Kaciulis, G. Mattogno, A. Mironas, V. Olevano, D. Senuliene & A. Setkus. Sensors and Actuators B: Chemical, vol. 43, page 140, 1997.

[Gatti 07a] M. Gatti. *Correlation effects in valence electron spectroscopy of transition metal oxides: many-body perturbation theory and alternative approaches*. PhD thesis, École Polytechnique, Palaiseau, November 2007.

[Gatti 07b] M. Gatti, F. Bruneval, V. Olevano & L. Reining. *Understanding correlations in vanadium dioxide from first principles*. Phys. Rev. Lett., vol. 99, page 266402, 2007.

[Gatti 07c] M. Gatti, V. Olevano, L. Reining & I. V. Tokatly. *Transforming Nonlocality into a Frequency Dependence: A Shortcut to Spectroscopy*. Phys. Rev. Lett., vol. 99, page 057401, 2007.

[Georges 96] A. Georges, G. Kotliar, W. Krauth & M. J. Rozenberg. Rev. Mod. Phys., vol. 68, page 13, 1996.

[Godby 87] R. W. Godby, M. Schlüter & L. J. Sham. Phys. Rev. B, vol. 35, page 4170, 1987.

[Gonze 09] X. Gonze*et al.* *http://www.abinit.org*, 1998-2009.

[Gross 85] E. K. U. Gross & W. Kohn. Phys. Rev. Lett., vol. 55, page 2850, 1985.

[Gross 03] E. K. U. Gross. *Public communication, San Sebastian Nanoquanta workshop*, 2003.

[Haug 96] H. Haug & A.-P. Jauho. Quantum kinetics in transport and optics of semiconductors. Springer, Berlin, 1996.

[Hedin 65] L. Hedin. *New method for calculating the one-particle Green's function with application to the electron-gas problem*. Phys. Rev., vol. 139, page A796, 1965.

[Hohenberg 64] P. Hohenberg & W. Kohn. Phys. Rev., vol. 136, page B864, 1964.

[Holm 98] B. Holm & U. von Barth. Phys. Rev. B, vol. 57, page 2108, 1998.

[Hybertsen 85] M. S. Hybertsen & S. G. Louie. Phys. Rev. Lett., vol. 55, page 1418, 1985.

[Kadanoff 62] L. P. Kadanoff & G. Baym. Quantum statistical mechanics. Benjamin, New York, 1962.

[Keldysh 64] L. V. Keldysh. Zh. Eksp. Teor. Fiz., vol. 47, page 1515, 1964.

[Kim 08] S. Kim, J. Ihm, H. J. Choi & Y.-W. Son. Phys. Rev. Lett., vol. 100, page 176802, 2008.

[Kittel 66] C. Kittel. Introduction to solid state physics. New York, 1966.

[Kohn 65] W. Kohn & L. J. Sham. Phys. Rev., vol. 140, page A1133, 1965.

[Korotin 02] M. A. Korotin, N. A. Skorikov & V. I. Anisimov. Phys. Met. Metallogr., vol. 94, page 17, 2002.

[Laad 06] M. S. Laad, L. Craco & E. Müller-Hartmann. Phys. Rev. B, vol. 73, page 195120, 2006.

[Lautenschlager 87] P. Lautenschlager, M. Garriga, L. Viña & M. Cardona. Phys. Rev. B, vol. 36, page 4821, 1987.

[Levy 82] M. Levy. Phys. Rev. A, vol. 26, page 1200, 1982.

[Liebsch 05] A. Liebsch, H. Ishida & G. Bihlmayer. Phys. Rev. B, vol. 71, page 085109, 2005.

[Mahan 89] G. D. Mahan & B. E. Sernelius. Phys. Rev. Lett., vol. 62, page 2718, 1989.

[Marinopoulos 02] A. G. Marinopoulos, L. Reining, V. Olevano, A. Rubio, T. Pichler, X. Liu, M. Knupfer & J. Fink. Phys. Rev. Lett., vol. 89, page 076402, 2002.

[Marinopoulos 04] A. G. Marinopoulos, L. Reining, A. Rubio & V. Olevano. Phys. Rev. B, vol. 69, page 245419, 2004.

[Meir 92] Y. Meir & N. S. Wingreen. *Landauer formula for the current through an interacting electron region.* Phys. Rev. Lett., vol. 68, page 2512, 1992.

[Neto 09] A. H. Castro Neto, F. Guinea, N. M. Peres, K. S. Novoselov & A. K. Geim. Rev. Mod. Phys., vol. 81, page 109, 2009.

[Olevano 98] V. Olevano*et al.* *http://www.dp-code.org*, 1998.

[Olevano 99a] V. Olevano, M. Palummo, G. Onida & R. Del Sole. *Exchange and Correlation Effects beyond the LDA on the Dielectric Function of Silicon.* Phys. Rev. B, vol. 60, page 14224, 1999.

[Olevano 99b] Valerio Olevano. *Proprietà Dielettriche di Semiconduttori oltre l'Approssimazione di Densità Locale.* PhD thesis, Università di Roma "Tor Vergata", Rome, March 1999.

[Olevano 00] V. Olevano, G. Onida & R. Del Sole. *Phenomenological Approximations to the Self-Energy Operator by a Generalized Xα method.* Phys. Rev. B, vol. 61, page 1912, 2000.

[Olevano 01] V. Olevano & L. Reining. *Excitonic Effects on the Silicon Plasmon Resonance.* Phys. Rev. Lett., vol. 86, page 5962, 2001.

[Park 07] C.-H. Park, F. Giustino, M. L. Cohen & S. G. Louie. Phys. Rev. Lett., vol. 99, page 086804, 2007.

[Redner 05] S. Redner. *Citation statistics from 110 years of Physical Reviews*. Physics Today, no. 58, page 49, 2005.

[Reining 02] L. Reining, V. Olevano, A. Rubio & G. Onida. *Excitonic Effects in Solids Described by Time-Dependent Density Functional Theory*. Phys. Rev. Lett., vol. 88, page 066404, 2002.

[Rotenberg 08] E. Rotenberg*et al.* Nature Materials, vol. 7, page 258, 2008.

[Runge 84] E. Runge & E. K. U. Gross. Phys. Rev. Lett., vol. 52, page 997, 1984.

[Schwinger 61] J. Schwinger. J. Math. Phys., vol. 2, page 407, 1961.

[Sham 83] L. J. Sham & M. Schlüter. Phys. Rev. Lett., vol. 51, page 1888, 1983.

[Sottile 03a] F. Sottile. *Response functions of semiconductors and insulators: from BSE to TDDFT*. PhD thesis, École Polytechnique, Palaiseau, September 2003.

[Sottile 03b] F. Sottile, V. Olevano & L. Reining. *Parameter-Free Calculation of Response Functions in Time-Dependent Density-Functional Theory*. Phys. Rev. Lett., vol. 91, page 056402, 2003.

[Sottile 07] F. Sottile, M. Marsili, V. Olevano & L. Reining. *Efficient ab initio calculations of bound and continuum excitons in the absorption spectra of semiconductors and insulators*. Phys. Rev. B, vol. 76, page 161103(R), 2007.

[Spataru 04] C. D. Spataru, L. X. Benedict & S. G. Louie. Phys. Rev. B, vol. 69, page 205204, 2004.

[Stiebling 78] J. Stiebling. Z. Phys. B, vol. 31, page 355, 1978.

[Sturm 92] K. Sturm, W. Schülke & J. R. Schmitz. *Plasmon-Fano resonance inside the particle-hole excitation spectrum of simple metals and semiconductors*. Phys. Rev. Lett., vol. 68, no. 2, pages 228–231, Jan 1992.

[Tokatly 01] I. V. Tokatly & O. Pankratov. Phys. Rev. Lett., vol. 86, page 2078, 2001.

[Trevisanutto 08] P. E. Trevisanutto, C. Giorgetti, L. Reining, M. Ladisa & V. Olevano. *Ab Initio GW Many-Body Effects in Graphene*. Phys. Rev. Lett., vol. 101, page 226405, 2008.

[van Leeuwen 98] R. van Leeuwen. Phys. Rev. Lett., vol. 80, page 1280, 1998.

[von Barth 05] U. von Barth, N. E. Dahlen, R. van Leeuwen & G. Stefanucci. *Conserving approximations in time-dependent density functional theory*. Phys. Rev. B, vol. 72, page 235109, 2005.

[Weissker 06] H. C. Weissker, J. Serrano, S. Huotari, F. Bruneval, F. Sottile, G. Monaco, M. Krisch, V. Olevano & L. Reining. *Signatures of Short-Range Many-Body Effects in the Dielectric Function of Silicon for Finite Momentum Transfer*. Phys. Rev. Lett., vol. 97, page 237602, 2006.

[Wentzcovitch 94] R. M. Wentzcovitch, W. W. Schulz & P. B. Allen. Phys. Rev. Lett., vol. 72, page 3389, 1994.

[Wiser 63] N. Wiser. Phys. Rev., vol. 129, page 62, 1963.

[Zhou 07] S. Y. Zhou, G.-H. Gweon, A. V. Fedorov, P. N. First, W. A. de Heer, D.-H. Lee, F. Guinea, A. H. Castro Neto & A. Lanzara. Nature Materials, vol. 6, page 770, 2007.

[Zhou 08] S. Y. Zhou*et al.* Nature Materials, vol. 7, page 259, 2008.

[Zylbersztejn 75] A. Zylbersztejn & N. F. Mott. Phys. Rev. B, vol. 75, page 4383, 1975.